

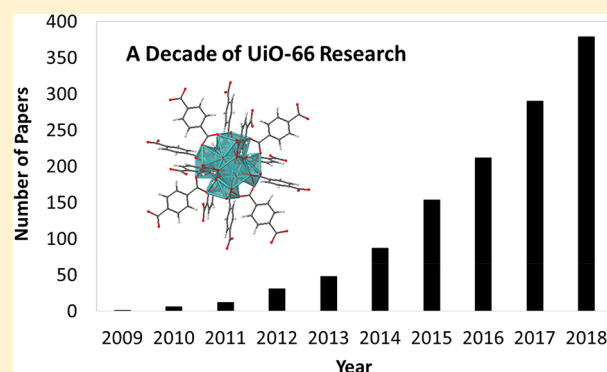
# A Decade of UiO-66 Research: A Historic Review of Dynamic Structure, Synthesis Mechanisms, and Characterization Techniques of an Archetypal Metal–Organic Framework

Joseph Winarta,<sup>†</sup> Bohan Shan,<sup>†</sup> Sean M. McIntyre,<sup>†</sup> Lei Ye,<sup>‡</sup> Cheng Wang,<sup>‡</sup> Jichang Liu,<sup>\*,‡</sup> and Bin Mu<sup>\*,‡</sup>

<sup>†</sup>School for Engineering of Matter, Transport, and Energy, Arizona State University, 501 East Tyler Mall, Tempe, Arizona 85287, United States

<sup>‡</sup>State Key Laboratory of Chemical Engineering, East China University of Science and Technology, Shanghai 200237, China

**ABSTRACT:** UiO-66 is an archetypal metal–organic framework (MOF) with a very high surface area as well as high thermal stability. It is found that the stability can be attributed to the metal oxide node being cuboctahedral allowing for 12 extension points for 1,4-benzenedicarboxylic acid (BDC) coordination. Because of this and its exceptional tunability and functionality, which are largely due to defect control of both missing-cluster and missing-linker defects, UiO-66 has gained scientific popularity. The combination of these characteristics allows for a highly versatile material that can be adapted to many different applications. The purpose for this work is to provide a historic overview of UiO-66, outlining the major developments that changed the synthesis strategies of Zr-based MOF as well as current and future works, which include defect control, aqueous crystallization, functionality–stability trade-offs, and advanced topographies. A breakdown of the various UiO-66 structures, including isorecticular and reo-type, and different characterization techniques such as powder X-ray diffraction, Fourier transform infrared spectroscopy, thermogravimetric analysis, and nitrogen porosimetry are discussed as well.



## 1. INTRODUCTION

Metal–organic frameworks (MOFs) have been under extensive academic study over the past 20 years and are emerging on the industrial scale.<sup>1</sup> Incredible surface area, tunable functional groups, and an atomic-level control over pore structure are among the properties that make these materials promising candidates for a variety of applications. Currently, when searching the keyword metal–organic framework and MOF in the Web of Science, there are more than 14 000 hits. However, research on MOF structures is not equal as only a handful of MOFs are at the center of most of these works. In this work, we loosely define archetypal MOFs as MOFs listed as the topic of over 1000 papers in the Web of Science database; a significant drop-off in this metric is observed below 1000. Figure 1 contains a survey of MOFs and the number of times that each of these is listed as a topic in Web of Science; ZIF-8, Mil-101, MOF-5, HKUST-1, and UiO-66 each meet this definition of archetypal MOFs. Each of these MOFs contains some combination of the following attributes that have naturally qualified them for the increased attention: easy synthesis, high relative stability, and/or benchmark properties in one or more applications. In addition, each one has unique traits, synthesis considerations, and structural analogues deserving of independent consideration.

The archetypal MOF UiO-66 is the focus of this review. Originally reported by Lillerud's group a decade ago,<sup>2</sup> it was first synthesized in the University of Oslo, so it is named after the university. A steadily increasing research interest has surrounded this MOF. Figure 2 contains the number of times UiO-66 is listed as the topic of a paper in the Web of Science database by year. The steady increase in both publications and understanding of UiO-66 has provided many fascinating research avenues in synthesis–structure relationships that are nearing maturity, while constantly revealing even more challenges and opportunities. A perspective focused on methodologies for synthesizing UiO-66 membranes and isorecticular structures, and potential scalable techniques, has recently been presented;<sup>3</sup> however, this work will focus on the synthesis–structure relationships and only present essential elements of topics that overlap with topics emphasized in their work. Other two recent reviews covered the applications of Zr-based MOFs in drug delivery and biomedicine,<sup>4</sup> and heterogeneous catalysis.<sup>5</sup> The goal of this review is to observe the progression of this Zr-based MOF and the evolution of the synthesis procedure.

Received: July 19, 2019

Published: December 11, 2019

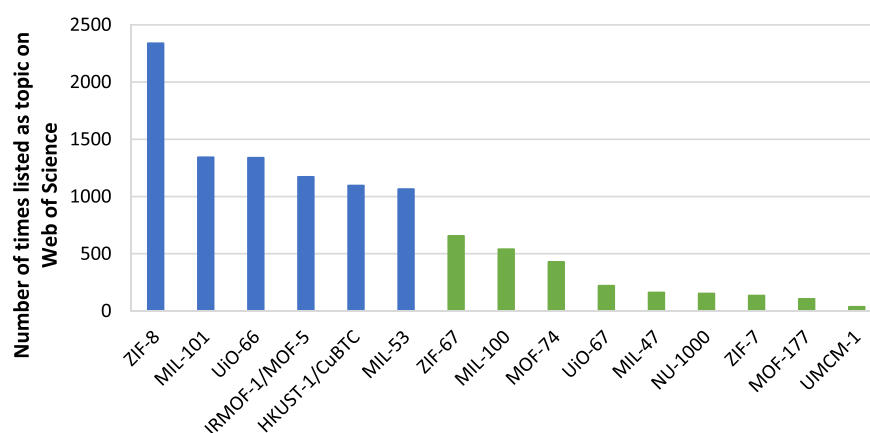


**Figure 1.** A selection of MOFs and the number of times each is listed as the topic to a paper in the Web of Science. Blue bars indicate benchmark MOFs, and green bars represent other MOFs.

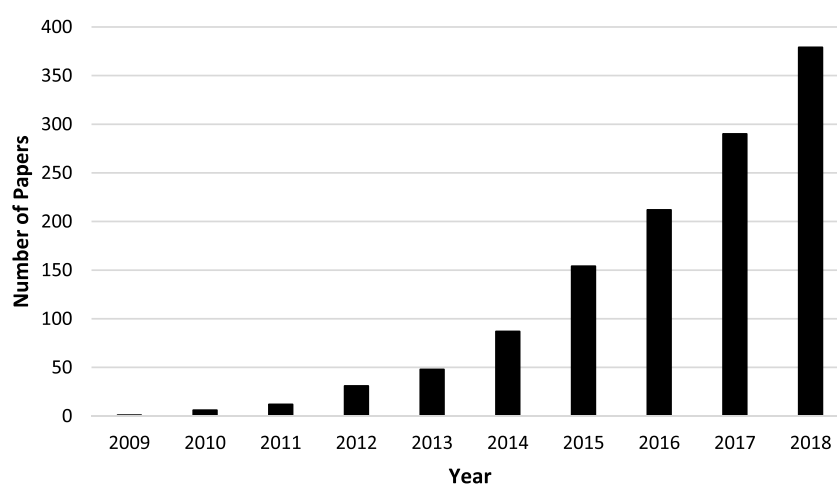


**Figure 2.** A survey of the number of papers found in the Web of Science database that lists UiO-66 as the topic of the paper.

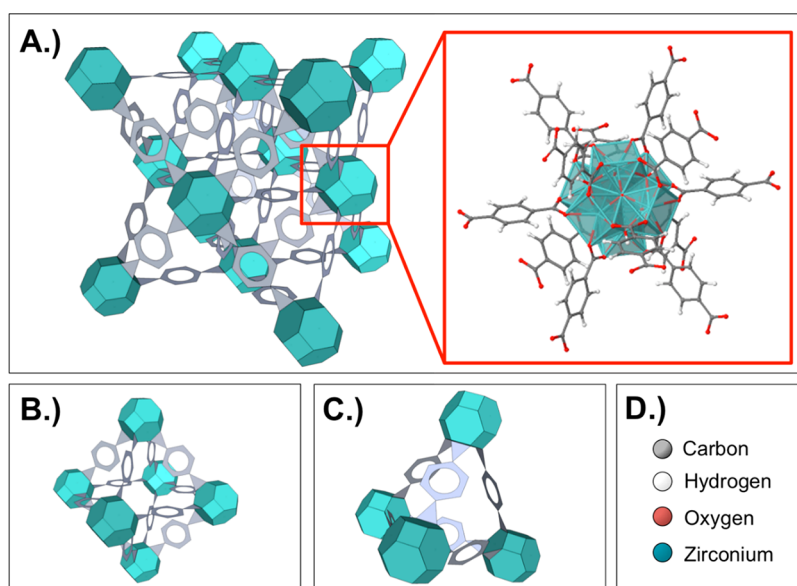


**Figure 3.** A representation of the UiO-66 structure. (A) The face-center-cubic UiO-66 structure composed of the metal node (aqua) and ligand (gray) with an atomic representation of the node and 12-connected terephthalic acid linkers from crystallographic data provided by Valenzano et al. in the Cambridge Crystallographic Data Centre<sup>9</sup> and generated from a visualizer using JSmol software at [www.crystal.unito.it/vibs/uio66\\_hydro/](http://www.crystal.unito.it/vibs/uio66_hydro/). (B) The node and ligand structure composing the 12 Å UiO-66 cage. (C) The node and ligand structure composing the 7.5 Å cage. (D) The color scheme for the atomic representation.

UiO-66 has received considerable attention due to an easy lab-scale synthesis, high relative stability, and leading properties for a variety of applications. The apparent thermodynamic stability of UiO-66 that is provided by the strong Zr–O bond has provoked excitement; in fact, it has been found that the carbon–carbon bonds in the ligand break down before the coordination bond.<sup>2</sup> Furthermore, UiO-66 has demonstrated superior mechanical,<sup>6</sup> thermal, acidic, aqueous, and water vapor stability. In terms of benchmark performance, the zirconium oxide node has proven to have unprecedented catalytic properties,<sup>7</sup> and the overall stability and porosity have enabled UiO-66 to perform in aqueous applications such as pervaporation and dye adsorption. It is synthesized on the lab-scale with an easy single-pot solvothermal synthesis and is also very reproducible in terms of adsorption properties.<sup>8</sup> These promising properties have led to numerous studies focused on understanding the synthesis–structure–property relationships of this material.

In this review, we focus on the current fundamental understanding of the synthesis, structure, and characterization of UiO-66. The following areas of research are discussed:

- **UiO-66 Structure and Characterization:** The structure of UiO-66 is discussed along with the dynamic changes between the hydroxylated and dehydroxylated form.
- **Evolution of UiO-66 Synthesis:** A progressive review of the synthesis of UiO-66 including the ingredients, main mechanisms, and factors that control defects, particle size, particle morphology, and intergrowth follow. A second section based on one of the most unique structural aspects of the UiO-66, defects, is also emphasized. Analytical techniques for characterizing these structural phenomena are also presented.
- **Isorecticular UiO-66 structures:** Essential elements of UiO-66 derivatives including both change to the metal and the ligand created through both isorecticular synthesis and postsynthetic modification are summarized.
- **Emerging Synthesis-Structure Research for the Next Decade:** In this section, we discuss recent papers that introduce new and potentially transformative UiO-66 synthesis and structure questions or discoveries that may catalyze the next decade of UiO-66 research.
- **Applications:** A summary of standard applications related to Zr-based MOFs as well as some emerging advanced applications.

## 2. UIO-66 STRUCTURE

UiO-66 is a crystal containing metal nodes composed of a zirconium oxide complex bridged by terephthalic acid ligands. Terephthalic acid is 1,4-benzenedicarboxylic acid (abbreviated as BDC). A representation of this structure is shown in Figure 3.

In its most stable form, called the hydroxylated form, this crystal is a face-centered-cubic structure containing an  $fm\bar{3}m$  symmetry with a lattice parameter of 20.7 Å.<sup>2</sup> It contains two separate cages, a tetrahedron cage of 7.5 Å, another an octahedron cage of 12 Å, and a pore aperture of 6 Å.<sup>9</sup> The theoretical pore volume of UiO-66 is 0.77 cm<sup>3</sup>/g, and the surface area is 1160 m<sup>2</sup>/g.<sup>10,11</sup> Yaghi and co-workers have developed a classification system called the Reticular Chemistry Structure Resource (RCSR),<sup>12</sup> and its use is strongly encouraged by IUPAC.<sup>13</sup> According to this terminology, UiO-66 is of the *fcu* topology. The use of this system for

MOFs includes defining the inorganic node as a secondary building unit (SBU)<sup>14</sup> and classifying the zirconium oxide node in UiO-66 as cuboctahedral, allowing up to 12 points of extension for BDC struts to coordinate.<sup>15</sup> Half of the eight oxygen atoms in the hydroxylated version of this SBU are bound to three zirconium atoms as individual atoms, and the remaining oxygen atoms are bound to three zirconium atoms in hydroxide form.

The dehydroxylated and hydroxylated states arise reversibly through the release or uptake of water molecules, respectively. To form the hydroxylated state, two oxygen atoms leave the SBU with the hydrogen atoms, leaving behind six oxygen atoms on the SBU, each coordinated to three zirconium atoms. This state may be induced by heating to 300 °C.<sup>2</sup> Valenzano et al. further studied the dehydroxylated state and observed that upon dehydration the node preferentially squeezes in one direction, but that these nodes squeeze in random directions over the entire structure still resulting in  $fm\bar{3}m$  symmetry.<sup>9</sup> Disagreement exists between the symmetry of the dehydroxylated species; the literature has also reported a preferential distortion over the entire crystal resulting in an  $R\bar{3}m$  symmetry;<sup>16</sup> however, currently the consensus appears to favor the  $fm\bar{3}m$  solution.<sup>10</sup> Chapman and co-workers note that structural phase transitions are also commonly seen in bulk zirconium oxide at much higher temperatures, dehydration and phase transitions are coupled but not directly linked, and UiO-66 dehydration initiates below 100 °C using in situ X-ray scattering techniques at Argonne National Lab.<sup>17</sup> Valenzano et al. demonstrate multiple characterization techniques that may be used to elucidate the difference between the hydroxylated and dehydroxylated node including PXRD and FTIR (Figure 4).<sup>9</sup>

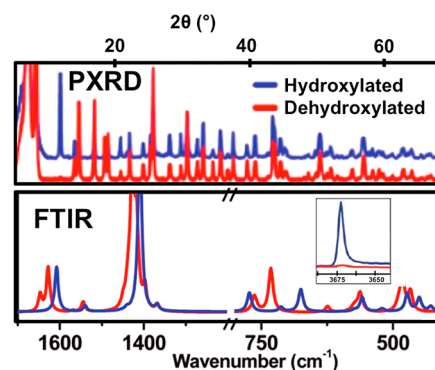


**Figure 4.** Demonstration of the characterization techniques that may be used to differentiate between the hydroxylated and dehydroxylated state. Reprinted with permission from Valenzano et al. Disclosing the complex structure of the UiO-66 metal organic framework: A synergic combination of experiment and theory. Reprinted from ref 9 with permission. Copyright 2011 American Chemical Society.

A full list of the theoretical FTIR peaks and their corresponding stretches for both the hydroxylated and dehydroxylated case may be found in the literature.<sup>9</sup> Llewellyn's group corroborates these differences in the FTIR spectra by monitoring the peak changes during increasing temperatures and finds a nearly complete disappearance of the –OH stretch at 3675 cm<sup>−1</sup> at 500 °C and states that they observe the same FTIR modifications as depicted in Figure 4.<sup>16</sup>

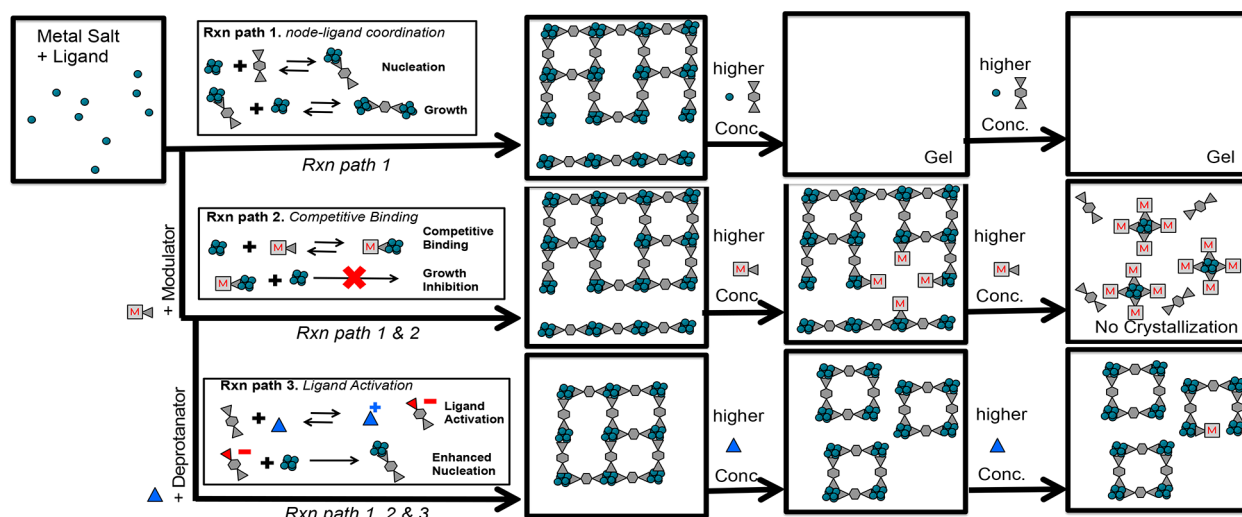


Figure 5. Summary of mechanisms involved in UiO-66 crystallization and related products.

Table 1. Survey of Recipes Highlighting Different Ingredients Including Original Uses of Modulators/Deprotonates<sup>a</sup>

metal salt	ligand (BDC)	solvent	time/temp	modulator	deprotonator	S.A. (m <sup>2</sup> /g)	ref
ZrCl <sub>4</sub> * 0.227 mmol	0.227 mmol*	DMF 24.9 mL 340 mmol	24 h 120 °C			1187	2
ZrCl <sub>4</sub> 0.343 mmol	0.343 mmol	DMF 20 mL 260 mmol	24 h 120 °C	AA* 10.29 mmol		1400	20
ZrCl <sub>4</sub> 1.53 mmol	1.53 mmol	DMF 21 mL 272 mmol	24 h 120 °C	AA 150 mmol		1188	27
ZrCl <sub>4</sub> 4 mmol	4 mmol	DMF 150 mL 1945 mmol	6 h 120 °C	AA 4 mmol	TEA* 1–8 mmol	1255–1315	21
ZrCl <sub>4</sub> 0.5 mmol	0.5 mmol	DMF 30 mL 390 mmol	24 h 100 °C	FA 50 mmol		1890	28

<sup>a</sup>A (\*) indicates that this work was the first to report UiO-66 synthesis, the use of modulator, or the use of a deprotonator.

### 3. EVOLUTION OF ZR-BASED MOF SYNTHESIS

**3.1. Early Stages.** Early synthesis strategies of UiO-66 involved highly dilute metal and ligand concentrations, without modulators or deprotonating agents.<sup>18,19</sup> Karl Petter Lillerud and co-workers first reported the synthesis procedure<sup>2</sup> of UiO-66 by mixing zirconium tetrachloride salt and terephthalic acid (H<sub>2</sub>BDC) and then dissolving in *N,N'*-dimethylformamide (DMF). The resulting mixture was then heated in a sealed container overnight. Crystallization occurred within the vessel, and after the allotted time, the solid was cooled, filtered, and washed repeatedly with DMF. As this was the first generation of Zr-based MOF, there was much exploring to do in terms of fine-tuning the recipe to achieve the best possible attributes as well as learning the mechanisms behind the synthesis. Without modulators or deprotonating agents, higher concentrations led to a rapid reaction that produces a gel product rather than powder MOFs. This results from rapid nucleation and interconnection, resulting in a 3D network without long-range order, which occurs due to the ligand dissociating from Zr cluster. The insufficient structural reparation leads to the amorphous product. A seminal work describing how modulators may be used as additives was presented by Schaate et al. in 2011,<sup>20</sup> and deprotonating agents were then introduced by Zhao et al.<sup>21</sup> A more detailed account of additives added to the UiO-66 crystallization reaction and the additional mechanisms they control is discussed.

**Modulator.** It is now understood that modulators may be used to competitively and reversibly bind to the metal node, slowing the crystallization process and allowing for crystal nucleation and a controlled growth. These modulators are often a single carboxylic acid connected to a carbon chain with the formula R-COOH,<sup>22</sup> where R may be a methyl group

(acetic acid, AA), hydrogen (formic acid, FA), a benzene ring (benzoic acid, BA), or even -CF<sub>3</sub> (trifluoroacetate, TFA).<sup>23,24</sup> These groups will bind to the metal node; however, because of a lack of a second carboxylic acid, the crystal structure will not propagate. This requires a balancing in the concentration of modulator added. If too much modulator is added, the crystallization may be entirely inhibited and will not occur. Another hypothesized impact of the modulator on the crystallization process is its impact on the hydrolysis of the zirconium.<sup>25</sup>

**Deprotonating Agents.** Deprotonating agents are useful for “activating” the ligands and initiating nucleation. Currently, the deprotonating agent used overwhelmingly in the literature is the base triethylamine (TEA).<sup>21,26</sup> Its function during MOF synthesis is to remove a hydrogen group from the BDC ligand to promote nucleation. However, with the addition of excessive deprotonation, it will also start to deprotonate the modulator and negate some of its intended effects.

A summary of the influence of each component on the crystallization is illustrated in Figure 5, and a table containing some representative recipes is given in Table 1. This table features works that are the first to report specific aspects of the UiO-66 synthesis recipe, along with a survey of a few other works to give a general idea of ideal concentration range and operating parameters. To provide a fair comparison between the effect of concentrations on recipes, only UiO-66 recipes that produce surface areas over 1000 m<sup>2</sup>/g are considered in this table. Recipes that push the borders of different operating parameters will be given in later sections.

This figure also shows that the modulator and deprotonating agent have influence over the crystal size and defects as well. This includes increased defects with increasing modulator, decreasing particle sizes with increasing deprotonating agent,



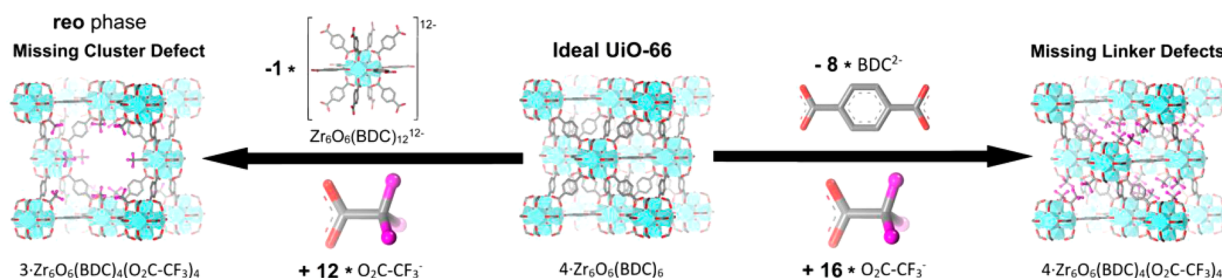


**Figure 6.** Image<sup>40</sup> distinguishing an ideal unit cell of UiO-66 and the two types of defects, missing-linker and missing-cluster, discussed above.

and defects at high concentrations of deprotonating agents. The causes for this, along with other controls over defects and morphology, are the next two topics.

From Table 1, it may be seen that the “default” operating parameters used for benchtop syntheses is at a temperature of 120 °C for 24 h, and solvent is typically *N,N*-dimethylformamide. The typical metal salt is  $\text{ZrCl}_4$ ; however, the use of  $\text{ZrOCl}_2$ ,<sup>29–31</sup>  $\text{ZrBr}_4$ ,<sup>31</sup>  $\text{Zr}(\text{OPr})_4$ ,<sup>31</sup> and  $\text{Zr}_6\text{O}_4(\text{OH})_4(\text{C}_6\text{H}_4\text{O}_4)_6$ <sup>31</sup> has also been reported. In addition, two other additives have also been used in academic literature, which are  $\text{HCl}$ <sup>23,32</sup> and water.<sup>23</sup>

The creation of the secondary building unit (zirconium oxide node) requires an oxygen source. This oxygen typically comes from three possible sources. It is either a part of the metal salt, stored in the *N,N*-dimethylformamide solvent, or directly added. Some zirconium salts come in hydrated states, and those that do not are typically extremely hygroscopic and become hydrated quickly. Water may also be stored on *N,N*-dimethylformamide or *N,N*-diethylformamide. Other groups have directly added small quantities of water (equimolar to the metal salt) to the reaction solution.<sup>23</sup> Although water could technically be considered another ingredient to UiO-66 crystallization, few works actually acknowledge it to date. Similarly, few works also consider mechanisms involving added water.<sup>20</sup> With the emergence of water as the primary solvent in the future, it seems likely that academic research will leapfrog a rigorous consideration of water as an additive.

**3.2. High-Quality Zr-Based MOF.** With the addition of modulators and deprotonation agents comes a new era of high-quality Zr-based MOFs being produced. The modulator provided exceptional control over the growth of the MOF and thus improved reproducibility and crystallinity. Decreased reaction time and other properties such as a well-defined shape, high thermal and moisture stability were also products of the introduction of modulators.<sup>25</sup> As these controlling agents gained popularity, interest in the science behind them built up and led to an explosion of papers studying these properties. These studies began to help researchers accumulate knowledge on the chemistry behind the modulators. Taddei et al. published a case study in which two different types of modulators are proposed.<sup>33</sup> The first type is coordination modulators. Coordination modulators (monocarboxylic acids) contest the organic ligand (BDC) for cluster coordination and ultimately allow for larger crystal growth by slowing the rate of precipitation. This is important because control over the MOF crystal size is vital when it comes to performance. For example, larger crystals allow for more detailed structural characterization and thus grant better understanding to the crystals as a whole. On the other hand, smaller crystals are necessary for more practical purposes. The second type is protonation modulation which occurs with the addition of a strong

inorganic acid, typically  $\text{HCl}$ , that slows the rate of precipitation by inhibiting the  $\text{H}_2\text{BDC}$  dissociation to BDC. This new generation of MOFs opened the door for much exploration in postsynthetic modification.

With this research boom on the second generation of Zr-based MOF, scientists found the material to not be very interesting as it is. The MOF was found to be very stable, but very inert, and thus its performance was not outstanding. However, these crystalline materials have an advantage over other porous materials such as zeolites: the organic ligand component. MOF organic linkers can be easily functionalized through a few different methods including direct solvothermal synthesis as well as postsynthetic approaches.<sup>34</sup> With this new step, MOFs became much more diverse in terms of their structure and functions. One type of modification proved to be the catalyst that propelled MOF research to the next level: defect engineering.

**3.3. Introduction of Defect Engineering.** UiO-66 is known for its high stability and coordination. This, however, could also be a drawback due to the inertness of the material because of these properties. The progressive goal to further enhance the functionality of MOFs has driven researchers to engineer the defects found within the material. These defects have been found to boost certain desirable properties such as a higher surface area and better adsorption properties. However, the defects also play a role in the decrease of its exceptional stability, effectively lowering crystallinity, increasing hydrophilicity, and increasing heat of adsorption.<sup>28</sup> Thus, a precise control over defects within the material is vital to its advanced development.

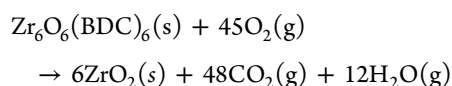
**Missing-Linker and Missing-Cluster Defects.** There are two possible types of defects in the UiO-66 structure: missing ligand<sup>35</sup> and missing cluster.<sup>28,36</sup> UiO-66 is a unique structure due to the possibility of the metal node coordinating with up to 12 ligand struts. This high degree of coordination allows multiple ligands to be omitted while still allowing the remaining ligands to provide enough structural support to the crystal. Observations of the missing ligand defects occurred in the first report of the UiO-66 structure in which it was reported that the framework averaged only 11 of the possible 12 ligands attached to each node.<sup>2</sup> Increasing the concentration of these defects has been well documented to decrease both water and thermal resistance.<sup>37,38</sup> However, the presence of these defects provides increased functionality. Omission of linkers opens zirconium metal sites at the node, providing increased Lewis-acid sites that may be used for catalysis and adsorption.

Goodwin and co-workers observed missing cluster defects<sup>36</sup> a couple of years after missing ligand defects were observed. Increasing missing cluster defects enhances accessibility to the framework by providing both larger pores and surface areas.

Simulations show that missing cluster defects have a much higher influence on increasing UiO-66 surface area than missing ligand defects.<sup>39</sup> Each type of defect is illustrated in Figure 6. Debate over the counterion providing charge balance defects has been prevalent in the literature. It has been hypothesized that this counterion may be chlorine from the metal salt,<sup>37</sup> residual additives called modulators,<sup>23</sup> residual solvent,<sup>22</sup> and/or water.<sup>22</sup> A thorough study was performed by Trickett et al. on this controversy, and they conclude the only significant counterion found in their study is provided by water molecules.<sup>31</sup> However, other studies still contradict this claim, which is likely a result of different synthesis conditions. EDX has confirmed chlorine groups on UiO-66 samples synthesized with HCl,<sup>23</sup> and NMR has shown the presence of fluorinated modulators at defective sites.<sup>23</sup>

In lieu of providing a chronological account of defect research, this section is outlined to describe the pros and cons of the three defect characterization techniques most prevalent in research laboratories: powder X-ray diffraction (PXRD), thermal gravimetric analysis (TGA), and nitrogen porosimetry. Less accessible studies that have played key roles in defect characterization such as single-crystal XRD<sup>22,31</sup> and neutron diffraction,<sup>10</sup> which will be used as a comparison. There are a few other techniques<sup>37</sup> that provide signatures of defects including FTIR (multiple –OH stretches), Raman spectroscopy (unexpected splits and weakened fingerprint region), and elemental analysis techniques that probe for species such as modulators or chlorine sitting at the defect sites. However, these methods are not yet widely used or developed.

**Thermal Gravimetric Analysis (TGA).** Defects were originally analyzed with TGA to observe missing linker defects. UiO-66 TGA curves demonstrate three distinct segments. First solvent loss is observed, and this is followed by dehydroxylation of the metal node. A final decomposition of the dehydroxylated UiO-66 structure is observed around 500 °C according to the reaction:<sup>37</sup>



The only solids in this decomposition are the initial dehydroxylated framework ( $\text{Zr}_6\text{O}_6(\text{BDC})_6$ ) and the final metal oxide ( $6\text{ZrO}_2$ ). Because  $\text{Zr}_6\text{O}_6(\text{BDC})_6$  is 220% heavier than  $6\text{ZrO}_2$ , a plateau on the TGA curve of the dehydroxylated UiO-66 structure should be 220% the weight of the final  $\text{ZrO}_2$  metal oxide. Lillerud and co-workers conclude that normalizing the TGA data to the final  $\text{Zr}_6\text{O}_6$  product may then allow the level of defects to be predicted from the shortcoming of this plateau to the theoretical 220% mark. This is demonstrated in Figure 7.

Although this method is well-corroborated in the literature by most, and in fact neutron diffraction measurements have matched TGA data that predicted 1/12 of the ligands missing,<sup>10</sup> some have still raised concerns with these assumptions.<sup>10</sup> In one case, overpredictions have been observed, which is expected to be caused by excess unreacted ligand left in the structure.<sup>37</sup> In other cases, and in particular highly defective frameworks, the TGA method has been demonstrated to fall short of actual defect measurements. A particular concern comes from the potential ambiguities caused by missing-cluster defects. If defect levels are high enough to cause missing clusters, then the implicit assumption that the dehydroxylated structure should be 220% higher than

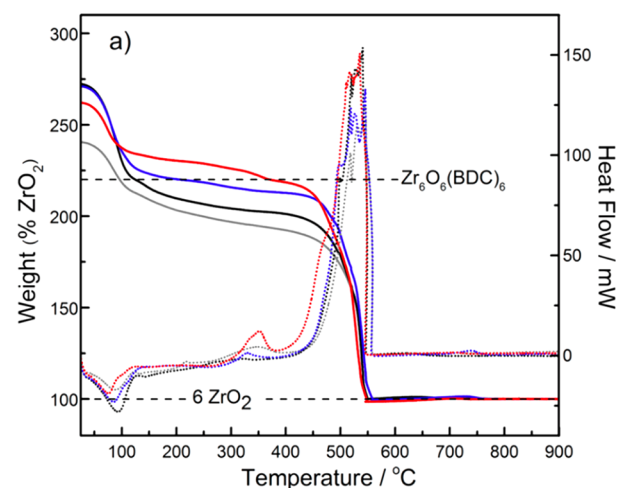


**Figure 7.** TGA curves for UiO-66 samples with varying degrees of defects from no defects (red), to some defects (blue), to more defects (black) to high defects (gray). The data show that if the weight is normalized to %  $\text{ZrO}_2$  the defects may be quantitatively determined by measuring the distance of the plateau near 400 °C from the 220% mark. Reprinted with permission from ref 37. Copyright 2014 American Chemical Society.

the final product is wrong. A second unknown is added to this formula, and missing clusters will result in missing ligands that go unaccounted for with this assumption.<sup>28</sup> However, our own work also has shown that this missing cluster issue is negligible when a small number of missing ligand defects are present, and in most cases a TGA quantification is in strong agreement with defect levels. Ease, reproducibility, and overwhelming validation over most of the defect range are undoubtedly why TGA has become the current gold-standard for defect quantification.

**Powder X-ray Diffraction (PXRD).** Missing cluster defects were seen using PXRD, a useful technique that differentiates between missing ligands and missing clusters.<sup>41</sup> Weak peaks are generated by an alternative crystalline phase with a differing topology of UiO-66 called reo morphology.<sup>42</sup> For the missing cluster defects, currently, people understand that the entire Zr cluster is missing from one-unit cell. This structure evolves into the reo-type structure. In a  $\text{ReO}_3$  (reo) morphology, Zr-clusters that are supposed to be sitting in the corners of the unit cell are missing.

The defective framework exhibits a broad peak at the lower angle from 4° to 6°, which are not presented in a simulated spectrum from the crystal structure. However, the current understanding toward these broad peaks is still insufficient. Waitschat et al. reported the systematic study<sup>43</sup> of UiO-66(Hf) revealing the defect formation is highly related to the presence of these peaks, but it is hard to quantitatively differentiate the contribution from each kind of defect.

**Nitrogen Porosimetry.** Study has revealed that another useful characterization method is the pore size distribution (PSD) of UiO-66, derived from the  $\text{N}_2$  adsorption isotherm. In pore size distribution data, the missing-ligand defects cause the pore diameter at around 6 Å shift to around 8 Å. This shift leads to the disappearance of the original peak, indicating that missing-ligand defects exist in the entire framework. Therefore, the formation of missing-ligand defects is a process driven by a coordination equilibrium shift. In the PSD data, the missing-cluster defects cause the new peak to appear from 15 to 20 Å.

**Table 2.** Collection and Summary of Studies Reporting Synthesis Procedures and Reaction Conditions Relating to Defects in UiO-66, where *M:L* Is the Coordination Modulator/Ligand Ratio, *S:L* Is Salt/Ligand Ratio, *t* Is Time, and *T* Is Temperature

studied parameter	characterization technique	description
<i>M/L</i>	pXRD	first synthesis of UiO-66 <sup>2</sup>
	pXRD, TGA	absence of 1/12 ligands in the system was first reported from TGA <sup>9</sup>
	pXRD, DLS, TGA	for UiO-66, showed that addition of coordination modulators results in individual (i.e., not intergrown) crystals via competitive coordination <sup>20,44</sup>
<i>t</i> , <i>M/L</i>	neutron powder diffraction	definitively showed the presence of ML defects using neutron powder diffraction <sup>10</sup>
<i>T</i> , <i>S/L</i>	pXRD, TGA	showed that the number of defects decreases with increasing <i>T</i> and <i>S/L</i> <sup>37</sup>
coordination modulator concentration	X-ray scattering	showed that missing-cluster defects occur in UiO-66 <sup>36</sup>
coordination modulator $pK_a$	BET	showed that the number of missing-cluster defects increases with the acidity (decreasing $pK_a$ ) of the modulator <sup>40</sup>
concentration of base comodulator	SEM	showed that the addition of a basic comodulator (TEA) to modulated synthesis solution results in monodispersed particles <sup>21</sup>
coordination modulator $pK_a$ , base comodulation, <i>T</i> , reactant concentration	BET, DLS	showed that the formation of missing-cluster defects can be explained by a partially deprotonated ligand mechanism <sup>28</sup>

Contrary to the missing-ligand defects peak, this peak is very broad, which depicts the presence of missing cluster defects in an adjacent manner.

These defects started to attract people's attention due to the largely increased surface area. The theoretical surface area of UiO-66 is around 1200 m<sup>2</sup>/g, and the defective framework has a much higher surface area around 1800 m<sup>2</sup>/g.<sup>28</sup> This interest led to the in-depth research on the factors that allow for the control of defects.

**Factors Influencing Defect Control.** Even though defectivity in UiO-66 is not yet fully understood, there have been many studies focused on synthesis procedures to systematically introduce defects into the structure. The following table lists some combinations of synthesis schemes and reaction conditions that have been reported in the literature.

The surface area of UiO-66 increases tremendously with increasing modulator. This parameter also increases with decreasing  $pK_a$  value of the modulator. After people realized this trend, trifluoroacetic acid started being used in generating defective frameworks, which led to surface areas reaching as high as 1800 m<sup>2</sup>/g. At the same modulator/ligand ratio, the sample synthesized with a modulator with a lower  $pK_a$  value has a higher surface area, but at first it was not fully understood how this relates to the number and type of defects.

As outlined in a recent paper from our group,<sup>28</sup> this result can be understood as follows: at the same modulator/ligand ratio, the UiO-66 synthesized with a modulator that has a lower  $pK_a$  value has more missing-cluster defects, and the UiO-66 synthesized with a modulator that has higher  $pK_a$  value has more missing-ligand defects. The  $pK_a$  value of a modulator depicts two things: (1) the capability of an acid to lose its proton, and (2) the strength of a conjugated base of the acid to bond with an empty orbital. Since the modulator with a smaller  $pK_a$  value dissociates more easily, there becomes an accumulation of protons in solution, impeding the deprotonation of ligands. There is ample evidence that the partially deprotonated ligands induce the formation of missing-cluster defects. Alternatively, the higher  $pK_a$  value modulator is more capable of association, and the shifted coordination equilibrium induced the formation of missing-ligand defects.

For the formation of missing-cluster defects, different groups have proposed different mechanisms. Cliffe et al. proposed that the formation of missing cluster defects is due to the concentration of deprotonated modulator attached on the Zr cluster.<sup>36</sup> Based on this hypothesis, the modulator cannot

accept another Zr cluster and thus form these defects. A modulator with low  $pK_a$  value is easier to form a deprotonated modulator, which makes the concentration of deprotonated modulator in the synthesis solution higher; therefore, a modulator with lower  $pK_a$  value can generate more defects. However, one problem with this mechanism is the low  $pK_a$  value modulator; the Zr-[Modulator]<sub>low pKa</sub> bond is weaker than the Zr-[Modulator]<sub>high pKa</sub> bond. For this reason, the proposed theory is based on partial deprotonation of the ligand due to accumulation of protons in solution.<sup>26</sup>

For the missing-ligand defects, the competitive relationship between [modulator] and [BDC] leads to the coordination equilibrium between Zr[Modulator] and Zr[Ligand]. Because of the existence of Zr[modulator], after the coordinated [modulator] is removed in the activation step, the defect-derived open metal sites can rejuvenate the activity of frameworks. Vermoortele et al. reported the catalysis activity of defective UiO-66 for Diels–Alder reactions.<sup>45,46</sup> Another way of using the missing-ligand defect is through the postsynthetic modification. Vandichel et al. carried out the compensating group substitution to replace the original coordinated modulator to more reactive groups to increase the framework activity.<sup>47</sup>

**Crystal Size, Morphology, and Intergrowth Control.** In UiO-66 synthesis, if the stability of UiO-66 is recognized as a result from the thermodynamically strong Zr-Ligand interaction, then the kinetic control of UiO-66 allows the governing of particle size, intergrowth, and orientation control. Toward the size control of UiO-66, the nucleation rate, number of nuclei, and the growth of each nucleus is examined. Through the control of these parameters, the particle size and particle size distribution can be manipulated.<sup>28</sup>

From a synthetic perspective, this discussion will focus on the effect of the modulator, deprotonating agent, and reactant concentration. After the addition of a modulator, this problem is effectively solved.<sup>26</sup> However, the BDC reaction rate between Zr is still much faster than the reaction metals like Zn and Cu. Therefore, the particle size of UiO-66 is intrinsically small. People may attribute the small particle size of UiO-66 to the fast reaction between Zr and ligand, which does not allow each nucleus to grow big enough; however, the actual situation is a little more complicated than this.

If the function of the modulator as a regulator is to control the reaction to improve the crystallinity, its particle size tuning



Table 3. Summary of UiO-66-R MOFs Reported in the Literature

UiO-66-R	UiO-66-(R) <sub>2</sub>	UiO-66-(R) <sub>4</sub>
<b>R</b> = NH <sub>2</sub> , <sup>31,57</sup> Br, <sup>31</sup> NO <sub>2</sub> , <sup>31</sup> OH, F, I, <sup>58</sup> CH <sub>3</sub> , SO <sub>3</sub> Na, <sup>58</sup> OCH <sub>3</sub> , COOH, <sup>58</sup> NO <sub>2</sub> , CF <sub>3</sub> , SO <sub>3</sub> H, C <sub>10</sub> H <sub>8</sub> .	<b>R, R'</b> = F, Cl, Br, OH, <sup>57</sup> SH, NH <sub>2</sub> , CH <sub>3</sub> , <sup>31</sup> OCH <sub>3</sub> , CF <sub>3</sub> , SO <sub>3</sub> H, COOH, <sup>57</sup> OCH <sub>2</sub> CH <sub>3</sub> . <sup>57</sup>	<b>R, R', R'', R'''</b> = F, <sup>57</sup> COOH. <sup>57</sup>

capability is an additional benefit. As a Zr cluster picks from either a modulator or a ligand to react, the reaction becomes competitive coordination. The addition of a modulator brings the local ligand association rate to a similar level as dissociation, and thus the global reaction rate between Zr and ligand is decreased. Therefore, the addition of a modulator will not only increase the crystallinity of UiO-66, but also increase the particle size of UiO-66. However, even though the  $pK_a$  value of the modulator is normally smaller than that of H<sub>2</sub>BDC, if the amount of modulator keeps increasing, there will be a point that the modulator reverses the direction of the reaction. The reaction will then end up as a clear solution rather than very large crystals. Therefore, solely adding modulator is not an effective way to produce large crystal.<sup>26</sup>

Since H<sub>2</sub>BDC and the modulators are organic acids, when they react with Zr, the protons remain in the liquid solution. Therefore, in a review of UiO-66 synthesis, these protons must be included in the discussion. The common lab scale synthesis is a batch-wise solvothermal synthesis. When the solvent amount is limited, the nature of weak acids (ligand and modulator) is stepwise deprotonation and partial deprotonation. Their presence can be found as H[modulator], [modulator], H<sub>2</sub>[BDC], H<sub>1</sub>[BDC], and [BDC]. The relative ratio among these components is governed by the  $pK_a$  value of each proton of modulator and H<sub>2</sub>BDC. The commonly used modulators in UiO-66 include trifluoroacetic acid, formic acid, acetic acid, and benzoic acid, which have  $pK_a$  values that are commonly smaller than H<sub>2</sub>BDC. Meanwhile, the amount of modulator added in the synthesis solution is more than 20 times of H<sub>2</sub>BDC. Hence, the large number of protons in synthesis solution can significantly impact the crystal growth as well.

Because of the high proton concentration and stepwise deprotonation of ligands, the synthesis solution will have a large concentration of partially deprotonated ligands. Its percentage will increase as the reaction proceeds. From a particle size point of view, the partially deprotonated ligand can function as surfactants to prevent the Ostwald ripening process.<sup>48</sup> In crystalline particle synthesis, the important process that leads to the homogeneous particle size is the Ostwald ripening process. The small size particle becomes the nutrition for the larger particles to keep growing. Therefore, along with the addition of a modulator, not only does the particle size become larger, the particle size distribution becomes more uniform.

For some other MOF research, the modulator addition is designed for the morphology control instead of the improving the crystallinity. The modulator or surfactants are used as a capping reagent. However, the morphology tuning of UiO-66

is rarely reported. The possible problems include the high symmetry of Zr clusters making it hard to have a facet to highly coordinate with the capping reagent. Another problem is that a Zr cluster with such a high coordination number has a higher tolerance toward the variation. Another possible reason is that the capping reagent needs to reach a certain coverage to see this variation. However, this coverage is hard to reach before protons start to be an obstacle. After the addition of the deprotonating agent, this modulator coverage is possible to reach.

The oriented growth of UiO-66 was reported by Miyamoto et al.<sup>49</sup> In their synthesis, acetic acid is used as the modulator, and water is used as the facilitating reagent. Acetic acid is a modulator with a relatively high  $pK_a$  value. Therefore, the coordination equilibrium tuning function of acetic acid is more obvious. Water may also serve as the buffer solution to diminish the accumulation of protons in the solution. When formic acid is used as the modulator and triethylamine is used as the deprotonating agent, the formic acid can lead to UiO-66 with 111 orientation and 200 orientation, as the intergrowth between the UiO-66 particles is impacted by the addition of modulator. The addition of a deprotonating agent or buffering solution can facilitate the intergrowth among UiO-66 crystals.

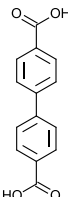
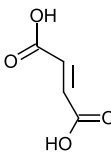
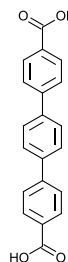
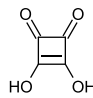
Intergrowth occurs when separate crystal networks join together physically but not chemically. The synthesis of continuous UiO-66 polycrystalline film is much less than the number of related studies in other MOFs. The partially deprotonated ligands impact the growth of UiO-66 from all levels. From the beginning, the partially deprotonated ligands cause the formation of missing-cluster defects as more protons accumulate in solution during the reaction process. This impact is so severe such that the intergrowth among UiO-66 particles is terminated by the partially deprotonated ligand; therefore, being able to remove the partially deprotonated ligand is important. Different from the normal UiO-66 synthesis method, the synthesis of UiO-66 film/membrane requires the addition of water. It is possible that the water can help to lower the impact from these protons. In another study, the deprotonating agent triethylamine is added to trigger the intergrowth between UiO-66 particles.<sup>26</sup> As long as the amount of TEA is enough to balance the protons, the intergrowth is independent from the modulator variation.

#### 4. ISORETICULAR UIO-66 STRUCTURES

One of the appealing aspects to UiO-66 is the broad range of structures within reach without drastic changes to synthesis procedures. Two primary routes exist for developing derivatives to the UiO-66 structure: isorecticular synthesis and postsynthetic modification. Each of these are very well



Table 4. Isorecticular UiO-66 Structures and Relevant Properties

Ligand	Structure Name/ Properties	Ligand	Structure Name/ Properties
	<b>UiO-67</b> Cage Size <sup>59</sup> : 16.0 Å Pore Aperture <sup>60</sup> : 8.0 Å Lattice Parameter <sup>61</sup> : 11.6 Å Surface Area <sup>62</sup> : 3000 m <sup>2</sup> /g		<b>ZrFMA</b> Cage Size <sup>63</sup> : 7.4 Å Pore Aperture <sup>64</sup> : 7 Å Lattice Parameter <sup>64</sup> : 17.9 Å Surface Area <sup>64</sup> : 856 m <sup>2</sup> /g
	<b>UiO-68</b> Cage Size <sup>20</sup> : 25.6 Å Pore Aperture <sup>65</sup> : 10.0 Å Lattice Parameter <sup>66</sup> : 15.2 Å Surface Area <sup>65</sup> : 4170 m <sup>2</sup> /g		<b>ZrSQU</b> Cage Size <sup>67</sup> : 5.6 Å Pore Aperture <sup>67</sup> : 2.4 Å Lattice Parameter <sup>67</sup> : 15.8 Å Surface Area <sup>67</sup> : 179 m <sup>2</sup> /g

presented in a recent review by Hu and Zhao,<sup>3</sup> and only the essential elements are presented here.

Isorecticular means the same topology, so an isorecticular synthesis means that a MOF composed of the same (SBU) and ligand coordination is used. When a new structure cannot be directly synthesized, postsynthetic processes such as solvent assisted ligand exchange (SALE) or metal exchange may be used. Metal substitutions to the UiO-66 structure are often noted as UiO-66(X), where the X is replaced by the atomic symbol of the metal; for instance, UiO-66 made with the hafnium metal is called UiO-66(Hf). In the literature, direct isorecticular synthesis of hafnium<sup>50</sup> and cerium<sup>51</sup> has been reported.

Isorecticular UiO-66 structures involving ligand exchanges are far more prevalent in the literature; there are two different types that are important. The first uses BDC with either one, two, or four functional groups replacing hydrogen atoms on the benzene ring. These UiO-66 analogues go by the name UiO-66-R, where the R represents the functional group. For example, if amine-functionalized BDC is used, the structure is called UiO-66-NH<sub>2</sub>, and if two of the hydrogen atoms on the benzene ring are replaced with an amine it would be named UiO-66-(NH<sub>2</sub>)<sub>2</sub>. A summary of UiO-66-R structures currently reported in the literature is given in Table 3. Mixed ligand structures using combinations of various functionalized BDC ligands have also been reported including BDC/ABDC<sup>52</sup> and BDC/BBDC,<sup>53</sup> and a combination of metal and ligand functionalization has been used to synthesize Ti(IV)/(NH<sub>2</sub>)<sub>2</sub>-BDC<sup>54</sup> and Ce/H<sub>2</sub>PZDC.<sup>55</sup>

The other type of UiO-66 isorecticular structures uses different bicarboxylic acid ligands, and most have been provided other numbers after the UiO designation. UiO-67 uses the 4,4'-biphenyl-dicarboxylate (BPDC) ligand, and UiO-68 uses the terphenyl dicarboxylate (TPDC) ligand. Others, including ZrFMA and ZrSQU, use the fumaric acid and squaric acid ligand, respectively. Table 4 contains a summary of various ligands that have been successfully used to create UiO-

66 isorecticular structures. A full review on reticular design, isorecticular expansion and contraction, catenation, and postsynthetic modification of Zr-MOFs was done by Farha and co-workers in a recent work.<sup>56</sup>

## 5. EMERGING SYNTHESIS-STRUCTURE RESEARCH FOR THE NEXT DECADE

UiO-66, as both a highly studied archetypal MOF and a benchmark MOF for a variety of applications, has the potential make a huge impact on the commercial scale. With a decade of research, much has been learned about the synthesis-structure relationship of this material, and proof-of-concept work for a variety of applications has certainly justified the potential of this fundamental UiO-66 research. A few emerging synthesis-structure research directions have the potential to finally push this material from its current academic intrigue into real commercial impact. Therefore, these research areas will be the focus of the next decade: aqueous crystallization, the functionality-stability trade-off, and advanced topographies. The current status of each of these research directions is discussed.

**Aqueous Crystallization.** Two realistic commercial MOF synthesis routes have recently been discussed by DeSantis et al.: solvent-assisted grinding and aqueous phase crystallization.<sup>68</sup> The goal of each of these synthesis routes is to maximize throughput while minimizing both energy input and solvent cost. BASF has demonstrated that aqueous phase crystallization may lead to production of MOFs on the ton scale if the material is water stable and reactants are water-soluble. Aqueous crystallization is likely the better of the two options for MOF meeting this criterion since current understanding of the crystallization process allows more control over crystal size and quality. Although few grinding studies have been performed, it is generally observed that the resulting product is of lower quality and yield than crystallization methods.

A study by Yang et al. demonstrated the first-ever synthesis of a UiO-66 derivative in an aqueous crystallization process, UiO-66-(COOH)<sub>2</sub>.<sup>69</sup> Reinch Yang et al. have provided a follow-up study of an aqueous UiO-66 synthesis as well.<sup>70</sup> In their work, they used Zr(SO<sub>4</sub>)<sub>2</sub> as the zirconium salt since it is water-soluble, limited their synthesis to below the boiling point of water to allow synthesis at atmospheric pressure, and avoided corrosive chemicals. They attempted to synthesize a series of UiO-66 analogues; however, in nearly all cases they observed a reduced ligand connectivity resulting in a body-centered cubic structure. The exception to this case was the synthesis of UiO-66-F<sub>4</sub>, which did contain the traditional face-centered cubic UiO-66 structure. Although the resulting frameworks did not have the traditional structure, they were still highly crystalline and appeared to contain regular defects and extra accessibility to the zirconium oxide node, which are undoubtedly interesting materials. In addition to this, Serre and co-workers found that the addition of both water and hydrochloric acid actually increased the rate of the reaction,<sup>71</sup> which was further supported by the work of Gascon and co-workers.<sup>72</sup> Hu et al. developed a modulated hydrothermal (MHT) synthesis technique involving a reflux reaction with a water/acetic acid solvent in which they have successfully synthesized several UiO-66-R type analogues.<sup>57</sup> This work was also repeated by Gray and co-workers in order to investigate the role of water in UiO-66(Zr/Hf) synthesis.<sup>73</sup> They found that increasing the concentration of water led to the emergence of the hexagonal close packing (hcp) material. This hcp phase gave a direct pathway to a highly crystalline hexagonal nanosheet (hns) phase through washing with a solvent and activation.

It is expected that more groundbreaking studies will be performed emphasizing the synthesis–structure properties of the aqueous crystallization of UiO-66 and its analogues in the coming decade. An increased understanding of this crystallization method undoubtedly may be the route to UiO-66 commercialization.

**Functionality-Stability Trade-Offs.** MOFs as a class of its own is a highly functional material due to their intrinsic porosity and large surface area as well as its outstanding tunability. The stability aspect did not come into play until the breakthrough of UiO-66 where high functionality met high stability.<sup>74</sup> Since then, many have contributed to this balance between two. Yuan et al. have recently published a work<sup>75</sup> outlining the current trends in group 4 metals and their impressive stability. The work highlights Zr, Ti, and Hf as the metals within these M<sup>IV</sup>-MOFs. In addition, bimetallic MOFs are also discussed as a possible solution around issues related to incompatibilities with formation conditions. On the other end of the spectrum, defect engineering has been a focal point in optimizing functionality in MOFs.<sup>76</sup> The consequences of these defects found in MOFs, however, are decreased thermal, mechanical, and structural stability.<sup>77</sup> These trade-offs will continue to be studied in the future to better optimize both factors for many different applications.

**Two-Dimensional Zr-Based MOFs.** Two-dimensional materials have been an area of incredible academic interest for years since the exfoliation of graphene from graphite in 2004.<sup>78</sup> The utility and scope of two-dimensional materials are vast, and they have great potential in a wide variety of fields; this is due to their unique structural features as well as unprecedented properties. Some benefits to ultrathin 2D nanomaterials include fascinating electronic properties due to

electron confinement, ultimate mechanical flexibility, optical transparency, high surface-to-volume atom ratios, and ultrahigh specific surface area.<sup>79</sup> MOFs have converged with this field, and the synthesis of a variety of topographies has already been pursued. Many 2D MOF nanosheet applications have been outlined in a work by Zhang and co-workers.<sup>80</sup> For gas separation, ultrapermeable and highly selective membranes<sup>81</sup> as well as mixed-matrix membranes (MMMs) have been reported.<sup>82</sup> For energy conversion and storage, because of their high surface-to-volume atom ratios, open metal sites are in abundance, allowing for their use in catalysis processes<sup>83</sup> and in lithium ion batteries.<sup>84</sup> Two-dimensional Zr-MOF nanosheets were found to aid in the detection of cocaine in an electrochemical sensor.<sup>85</sup> In addition, a Zr-based UiO nanoscale MOF was used to aid in a drug delivery process for cancer cells.<sup>86</sup> To date, only a few 2D zirconium-based MOFs have been reported. These include zirconium porphyrin,<sup>87</sup> zirconium BTB,<sup>88</sup> UiO-66 F<sub>4</sub>BDC,<sup>73</sup> UiO-66 nanosheets.<sup>89</sup> Some hafnium-based nanosheets have also been investigated, including HfBTB,<sup>90</sup> UiO-67(Hf),<sup>91</sup> and Hf<sub>6</sub>O<sub>4</sub>(OH)<sub>4</sub>(HCO<sub>2</sub>)<sub>6</sub>(BTB)<sub>3</sub>.<sup>92</sup> UiO-66 and its derivatives are likely to become much more impactful in this field in the near future.

## 6. APPLICATION

The primary application for metal–organic frameworks is gas adsorption with influence in storage, separation, and purification. Camille Petit compiled a review article in 2018 in which the most notable applications for both adsorption and molecular separation are highlighted.<sup>93</sup> This list includes acidic gas adsorption, toxic gas removal, gas storage, and water purification. A summary of the work can be found in Table 5.

**Table 5. Summary of Petit's Review Paper on Adsorption and Molecular Separation MOF Research<sup>93</sup>**

application	MOF	ref
CO <sub>2</sub> adsorption	Mg-MOF-74	94
SO <sub>2</sub> and NO <sub>2</sub> adsorption	MIL-125	95
CO removal	Cu <sub>3</sub> (btc) <sub>2</sub>	96
NH <sub>3</sub> removal	M <sub>2</sub> Cl <sub>2</sub> (BTDD)-(H <sub>2</sub> O) <sub>2</sub>	97
H <sub>2</sub> S removal	ZIF-8	98
H <sub>2</sub> O adsorption	MOF-801	99
H <sub>2</sub> storage	Mn-BTT	100
CH <sub>4</sub> storage	HKUST-1	101
O <sub>2</sub> /N <sub>2</sub> separation	Fe <sub>2</sub> (dobdc)	102
olefin/paraffin separation	M <sub>2</sub> (m-dobdc)	103
Kr and Xe adsorption/separation	SBMOF-1	104
water purification	Zr-based	105

For more advanced applications, some emerging research could prove to be groundbreaking in the years to come. These include different types of catalysis and doping processes, sensors, biomedicine, and toxic gas removal; some examples will be discussed below.

In a world where energy consumption has risen to new heights, the search for a sustainable energy source has been a very important and challenging task. One source of sustainable energy is the sun, which provides unlimited solar energy and thus has been the focal point of environmental science. Zhang et al. found that the research on MOFs used in photocatalytic reactions related to solar fuel production and organic synthesis have been lacking and thus have very high potential for future

works.<sup>106</sup> Currently, under photocatalytic conditions, most MOFs have mediocre stability; and those that can withstand such conditions have limited functionality within the system. Thus, in this study, it can be seen that there must be an advancement of research into photoactive metals as well as fluorescent ligands within certain MOFs as this will aid in the property control and ultimately better photocatalytic performance.

In a recent work by Garcia and co-workers, UiO-66 was analyzed for the use in catalysis.<sup>5</sup> Stability is a major concern for MOFs used in catalysis; however UiO-66, having one of the highest structural robustness, was one of several promising MOFs. Table 6 below outlines some catalysis reactions on

**Table 6. Catalysis Reactions on UiO-66 and Its Derivatives**

catalysis reaction	derivative
cyclization of citronellal to isopulegol <sup>145</sup>	defective UiO-66
CO <sub>2</sub> cycloaddition of styrene oxide <sup>107</sup>	ground/sieved UiO-66 powder
synthesis of pyrano[3,2-c]quinoline <sup>108</sup>	UiO-66 and UiO-66-NH <sub>2</sub>
conversion of ethyl levulinate to $\gamma$ -valerolactone (GVL) <sup>109</sup>	UiO-66(Zr), UiO-66-NH <sub>2</sub> , and UiO-66-COOH
transformation of cellulose to HMF <sup>110</sup>	UiO-66-SO <sub>3</sub> H
conversion of methyl levulinate to GVL <sup>111</sup>	UiO-66-SO <sub>3</sub> H
acetalization of benzaldehyde and Morita Baylis Hillman (MBH) reactions <sup>112</sup>	UiO-66-RARSO <sub>3</sub> H
multicomponent synthesis of dihydro-2-oxopyrroles <sup>113</sup>	UiO-66-SO <sub>3</sub> H
esterification of levulinic acid <sup>114</sup>	UiO-66-NH <sub>2</sub>
synthesis of jasminaldehyde <sup>114</sup>	UiO-66-NH <sub>2</sub>
ring opening reaction of styrene oxide by methanol <sup>115</sup>	UiO-66-Br

UiO-66. In almost all cases, the use of UiO-66 or one of its derivatives increased conversion and/or efficiency of the overall reaction.

Chemicals and chemical reactions can be found in almost every aspect of industrial processes and may produce harmful gases such as ammonia and carbon monoxide. Specialized chemical gas sensors are in high demand for the safety of workers and the longevity of the processes. Not only this, but an increase in environmental awareness has led to the increase in attention in this area. Because of the perpetual nature of the problem, the solution must be tunable to meet the countless needs that may arise. MOFs are the perfect candidate for this issue, and some research has already been done; however, there is still much room for growth. Li et al. have compiled information about the advancements of metal–organic frame-

works used for gas sensing.<sup>116</sup> Some notable entries include UiO-MOFs for sensing aldehydes under 100 ppb using a fluorescence sensing method, UiO-66 for sensing alcohols with absorbance peak shift and visible color change to the naked eye, and UiO-67 for detecting O<sub>2</sub> using phosphorescence with high quenching efficiency of 65% at 0.8 atm O<sub>2</sub>. Their large surface area, diverse pore structure, reversible adsorption/desorption and highly tunable functionalities, including selectivity, are all reasons why MOFs are the future in gas sensor systems.

MOFs have become an established material in material science due to its versatile nature; however, an unexpected area that MOFs have found themselves in is in the field of biomedicine. It is in the biodegradable character of certain metal–ligand combination structures that allows for the degradation of the MOF in body fluids with a very diverse time table of minutes to weeks.<sup>117</sup> This “BioMOF” opens up many possible avenues for drug delivery as well as contrast agents in optical imaging such as MRI and X-rays. In fact, recent studies have shown that zirconium-based MOFs are suitable for drug delivery systems (DDSs) due to their enhancements in aqueous stability, biocompatibility, colloidal dispersion, and stimuli-responsive drug release.<sup>4</sup> These enhancements are done through surface functionalization and postsynthetic modification. In addition, drug delivery applications can benefit from the tunable pore sizes of MOFs as many different active molecules can be encapsulated into the MOFs for delivery into the host.

MOFs have also proved to be a promising candidate in toxic gas removal systems such as those found in filtration and decontamination areas.<sup>118</sup> Gas masks also provide a wide range of chemical removal since a standard mask is used to protect the user from a variety of toxic gases.<sup>119</sup> This development has recently become more prevalent as there is a growing need to better protect people such as first responders. Similar to the previous examples, MOFs are a promising candidate in this growing field due to their tunable characteristics in which they can be synthesized and modified to a specific set in order to meet various needs. Filtration on a larger scale such as for industrial reactions and automobiles can also be in the scope of this material.<sup>96</sup> In addition to this, destruction of chemical warfare agents are also being studied.<sup>120–123</sup> However, this topic will be omitted from this work as more studies need to be conducted before it can be used on such a scale.

Lastly, doping is a strategy used on MOFs in order to functionalize them further. This can lead to the resulting composites having the combined advantages of their

**Table 7. Doping UiO-66 and Its Applications**

material	application enhancement
lanthanum-doped UiO-66 adsorbent <sup>125</sup>	greatly increased phosphate capture capacity at 348.43 mg g <sup>-1</sup>
titanium-doped UiO-66 adsorbent <sup>127</sup>	enhanced adsorption capacity for organic dye removal at 979 mg g <sup>-1</sup>
titanium-doped amine-functionalized UiO-66 <sup>128</sup>	achieved exceptional catalytic performance with a H <sub>2</sub> production rate of 42 000 mL h <sup>-1</sup> g <sup>-1</sup> from formic acid.
cobalt-doped UiO-66 nanoparticle <sup>126</sup>	high adsorption capacity of tetracycline at 224.1 mg g <sup>-1</sup>
europium-doped UiO-66 <sup>129</sup>	highly sensitive sensor that detects hydrazine hydrate at concentrations as low as 0.18 $\mu$ M in under 90 s
europium-doped UiO-66 <sup>130</sup>	luminescence sensor for Cd <sup>2+</sup> at concentrations as low as 0.22 $\mu$ M in under 5 min
cerium-doped UiO-66/graphene nanocomposites <sup>131</sup>	enhanced photocatalytic activity for the reduction of nitroaromatic compounds
cerium-doped UiO-66 nanocrystals <sup>132</sup>	efficiently remove organic dyes such as methylene blue (145.3 mg g <sup>-1</sup> ), methyl orange (639.6 mg g <sup>-1</sup> ), and congo red (826.7 mg g <sup>-1</sup> ) from aqueous solutions.
cerium-doped UiO-66 <sup>133</sup>	excellent NO <sub>2</sub> adsorption at 95 mg g <sup>-1</sup> in dry conditions and 53 mg g <sup>-1</sup> in conditions where water is present.



composition.<sup>124</sup> The doping agent will induce an impurity that changes its structural properties. This structural change can be finely tuned to meet the needs of its specific application. For example, Luo and co-workers synthesized novel lanthanum-doped UiO-66 for phosphate capture. Using XPS, the group found that the coordination between lanthanum and terephthalic acid dropped from seven-coordination to six-coordination, which effectively increased adsorption capacity of phosphate by exposing more adsorption sites.<sup>125</sup> Another example comes from Yang and co-workers, who synthesized a novel cobalt-doped UiO-66 photocatalytic adsorbent that captures tetracycline (TC) molecules. It was found that the doped cobalt greatly enhanced adsorption capacity as well as photocatalytic activity in UiO-66.<sup>126</sup> The group discerned that this was due to the  $\pi$ - $\pi$  interaction as well as the electrostatic interaction that occurred between the cobalt-doped UiO-66 nanoparticle and the TC molecules. Table 7 below outlines a number of doping UiO-66 applications that are found throughout the literature.

## 7. CONCLUSION

It has now been over a decade since UiO-66 was first developed, and this review has captured an overview of the progression of not only UiO-66, but Zr-based MOFs as a field. In this work, the structure of UiO-66 was first outlined in detail as well as the characterization techniques related. Second, the progressive history of UiO-66 development was discussed, broken into first-, second-, and third-generation Zr-based MOFs. Within this section, the usefulness of modulators and deprotonating agents was outlined as well as the groundbreaking tunability of defects found within the structure. Third, isorecticular structures were broken down, and it was found that these derivatives that bare the same topology as the original UiO-66 vastly increased the functionalization of this MOF by allowing for isorecticular synthesis and postsynthetic modification. Fourth, aqueous crystallization, the functionality–stability trade-off, and advanced topographies were discussed as the future of this field of research. Lastly, the applications of these MOFs were outlined and discussed in detail with comprehensive tables outlining many different applications found in literature. The highly tunable nature of this exceedingly stable MOF allows strategies such as doping and postsynthetic modifications to add functionalities for their specific applications. It is anticipated that this research will continue to advance into many different fields as there have been many exciting prospects for the application of UiO-66 in areas such as catalysis, photocatalysis, adsorption separation, sensors, and even in biomedicine. Many, if not all of the highlighted catalysis works have shown either an increase in conversion, efficiency, or both. In adsorption separation, many of the techniques are already being used in industrial processes but can still be improved on in the future. Some work, however, still needs to be done in some application areas such as sensors, biomedicine, and photocatalysis before UiO-66 can really be useful. In utilizing MOFs as chemical sensors, the challenge is signal transduction in MOFs such as color change and quenching. Additionally, developing highly stable, sensitive, and selective sensors at room temperature proves to still be a challenge. This is important since these chemical sensors will mostly be operating at room temperature for the benefit of the operator. In biomedicine, hydrothermal stability is proven; however, a systematic study on their liquid phase stability must still be done. Lastly, in photocatalysis, MOFs in general suffer

from poor photostability and thus degrade easily under this stress, which is why composites are widely used in this field. Further research must be conducted in order to improve these issues for their respective applications. In light of all this, the future of this material is still very bright, and many new discoveries will be made in the decades to come.

## AUTHOR INFORMATION

### Corresponding Authors

\*(B.M.) E-mail: [bmu@asu.edu](mailto:bmu@asu.edu).

\*(J.L.) E-mail: [liujc@ecust.edu.cn](mailto:liujc@ecust.edu.cn).

### ORCID

Bohan Shan: 0000-0001-5674-981X

Jichang Liu: 0000-0002-5295-1778

Bin Mu: 0000-0002-9117-1299

### Notes

The authors declare no competing financial interest.

## ACKNOWLEDGMENTS

B.M. would like to acknowledge the National Science Foundation (Grant Number CMMI-1825594). J.L. acknowledges the joint fund by the National Natural Science Foundation of China and PetroChina (Project U1862204).

## REFERENCES

- (1) Gaab, M.; Trukhan, N.; Maurer, S.; Gummaraju, R.; Müller, U. The progression of Al-based metal-organic frameworks - From academic research to industrial production and applications. *Micro-porous Mesoporous Mater.* **2012**, *157*, 131–136.
- (2) Cavka, J. H.; Jakobsen, S.; Olsbye, U.; Guillou, N.; Lamberti, C.; Bordiga, S.; Lillerud, K. P. A new zirconium inorganic building brick forming metal organic frameworks with exceptional stability. *J. Am. Chem. Soc.* **2008**, *130*, 13850–13851.
- (3) Hu, Z.; Zhao, D. De facto methodologies toward the synthesis and scale-up production of UiO-66-type metal-organic frameworks and membrane materials. *Dalt. Trans.* **2015**, *44*, 19018–19040.
- (4) Abánades Lázaro, I.; Forgan, R. S. Application of zirconium MOFs in drug delivery and biomedicine. *Coord. Chem. Rev.* **2019**, *380*, 230–259.
- (5) Dhakshinamoorthy, A.; Santiago-Portillo, A.; Asiri, A. M.; Garcia, H. Engineering UiO-66 Metal Organic Framework for Heterogeneous Catalysis. *ChemCatChem* **2019**, *11*, 899–923.
- (6) Wu, H.; Yildirim, T.; Zhou, W. Exceptional mechanical stability of highly porous zirconium metal-organic framework UiO-66 and its important implications. *J. Phys. Chem. Lett.* **2013**, *4*, 925–930.
- (7) Rimoldi, M.; Howarth, A. J.; Destefano, M. R.; Lin, L.; Goswami, S.; Li, P.; Hupp, J. T.; Farha, O. K. Catalytic Zirconium/Hafnium-Based Metal-Organic Frameworks. *ACS Catal.* **2017**, *7*, 997–1014.
- (8) Park, J.; Howe, J. D.; Sholl, D. S. How Reproducible Are Isotherm Measurements in Metal-Organic Frameworks? *Chem. Mater.* **2017**, *29*, 10487–10495.
- (9) Valenzano, L.; Civalieri, B.; Chavan, S.; Bordiga, S.; Nilsen, M. H.; Jakobsen, S.; Lillerud, K. P.; Lamberti, C. Disclosing the complex structure of UiO-66 metal organic framework: A synergic combination of experiment and theory. *Chem. Mater.* **2011**, *23*, 1700–1718.
- (10) Wu, H.; Chua, Y. S.; Krungleviciute, V.; Tyagi, M.; Chen, P.; Yildirim, T.; Zhou, W. Unusual and highly tunable missing-linker defects in zirconium metal-organic framework UiO-66 and their important effects on gas adsorption. *J. Am. Chem. Soc.* **2013**, *135*, 10525–10532.
- (11) Ghosh, P.; Colón, Y. J.; Snurr, R. Q. Water Adsorption in UiO-66: The Importance of Defects. *Chem. Commun.* **2014**, *50*, 11329–11331.



- (12) O'Keeffe, M.; Peskov, M. A.; Ramsden, S. J.; Yaghi, O. M. (RCRS) Database of, and Symbols for, Crystal. *Acc. Chem. Res.* **2008**, *41*, 1782–1789.
- (13) Batten, S. R.; Champness, N. R.; Chen, X.-M.; Garcia-Martinez, J.; Kitagawa, S.; Öhrström, L.; O'Keeffe, M.; Paik Suh, M.; Reedijk, J. Terminology of metal–organic frameworks and coordination polymers (IUPAC Recommendations 2013). *Pure Appl. Chem.* **2013**, *85*, 1715–1724.
- (14) Yaghi, O. M.; O'Keeffe, M.; Ockwig, N. W.; Chae, H. K.; Eddaoudi, M.; Kim, J. Reticular synthesis and the design of new materials. *Nature* **2003**, *423*, 705–714.
- (15) Furukawa, H.; Cordova, K. E.; O'Keeffe, M.; Yaghi, O. M. The chemistry and applications of metal–organic frameworks. *Science (Washington, DC, U. S.)* **2013**, *341*, 1230444.
- (16) Wiersum, A. D.; Soubeyrand-Lenoir, E.; Yang, Q. Y.; Moulin, B.; Guiller, V.; Ben Yahia, M.; Bourrelly, S.; Vimont, A.; Miller, S.; Vagner, C.; Daturi, M.; Clet, G.; Serre, C.; Maurin, G.; Llewellyn, P. L. An Evaluation of UiO-66 for Gas-Based Applications. *Chem. - Asian J.* **2011**, *6*, 3270–3280.
- (17) Platero-Prats, A. E.; Mavrandonakis, A.; Gallington, L. C.; Liu, Y.; Hupp, J. T.; Farha, O. K.; Cramer, C. J.; Chapman, K. W. Structural Transitions of the Metal-Oxide Nodes within Metal-Organic Frameworks: On the Local Structures of NU-1000 and UiO-66. *J. Am. Chem. Soc.* **2016**, *138*, 4178–4185.
- (18) Garibay, S. J.; Cohen, S. M. Isoreticular synthesis and modification of frameworks with the UiO-66 topology. *Chem. Commun.* **2010**, *46*, 7700–7702.
- (19) Kandiah, M.; Tilset, M.; Lillerud, K. P.; Svelle, S.; Usseglio, S.; Olsbye, U. Post-synthetic modification of the metal–organic framework compound UiO-66. *J. Mater. Chem.* **2010**, *20*, 9848.
- (20) Schaate, A.; Roy, P.; Godt, A.; Lippke, J.; Waltz, F.; Wiebcke, M.; Behrens, P. Modulated synthesis of Zr-based metal–organic frameworks: From nano to single crystals. *Chem. - Eur. J.* **2011**, *17*, 6643–6651.
- (21) Zhao, Y.; Zhang, Q.; Li, Y.; Zhang, R.; Lu, G. Large-Scale Synthesis of Monodisperse UiO-66 Crystals with Tunable Sizes and Missing Linker Defects via Acid/Base Co-Modulation. *ACS Appl. Mater. Interfaces* **2017**, *9*, 15079–15085.
- (22) Øien, S.; Wragg, D.; Reinsch, H.; Svelle, S.; Bordiga, S.; Lamberti, C.; Lillerud, K. P. Detailed structure analysis of atomic positions and defects in zirconium metal–organic frameworks. *Cryst. Growth Des.* **2014**, *14*, 5370–5372.
- (23) Vermoortele, F.; Bueken, B.; Le Bars, G.; Van de Voorde, B.; Vandichel, M.; Houthoofd, K.; Vimont, A.; Daturi, M.; Waroquier, M.; Van Speybroeck, V.; Kirschhock, C.; De Vos, D. E. Supporting information for Synthesis Modulation as a Tool To Increase the Catalytic Activity of Metal–Organic Frameworks: The Unique Case of UiO-66 (Zr). *J. Am. Chem. Soc.* **2013**, *135*, 11465–11468.
- (24) Bon, V.; Senkovska, I.; Weiss, M. S.; Kaskel, S. Tailoring of network dimensionality and porosity adjustment in Zr- and Hf-based MOFs. *CrystEngComm* **2013**, *15*, 9572–9577.
- (25) Ren, J.; Langmi, H. W.; North, B. C.; Mathe, M.; Bessarabov, D. Modulated synthesis of zirconium-metal organic framework (Zr-MOF) for hydrogen storage applications. *Int. J. Hydrogen Energy* **2014**, *39*, 890–895.
- (26) Shan, B.; James, J. B.; Armstrong, M. R.; Close, E. C.; Letham, P. A.; Nikkhah, K.; Lin, Y. S.; Mu, B. Influences of Deprotonation and Modulation on Nucleation and Growth of UiO-66: Intergrowth and Orientation. *J. Phys. Chem. C* **2018**, *122*, 2200–2206.
- (27) Armstrong, M. R.; Arredondo, K. Y. Y.; Liu, C. Y.; Stevens, J. E.; Mayhob, A.; Shan, B.; Senthilnathan, S.; Balzer, C. J.; Mu, B. UiO-66 MOF and Poly(vinyl cinnamate) Nanofiber Composite Membranes Synthesized by a Facile Three-Stage Process. *Ind. Eng. Chem. Res.* **2015**, *54*, 12386–12392.
- (28) Shan, B.; McIntyre, S. M.; Armstrong, M. R.; Shen, Y.; Mu, B. Investigation of Missing-Cluster Defects in UiO-66 and Ferrocene Deposition into Defect-Induced Cavities. *Ind. Eng. Chem. Res.* **2018**, *57*, 14233–14241.
- (29) Deria, P.; Bury, W.; Hupp, J. T.; Farha, O. K. Versatile functionalization of the NU-1000 platform by solvent-assisted ligand incorporation. *Chem. Commun.* **2014**, *50*, 1965–1968.
- (30) Wang, T. C.; Farha, O. K.; Stoddart, J. F.; Hupp, J. T.; Kim, I. S.; Martinson, A. B. F.; Vermeulen, N. A. Scalable synthesis and post-modification of a mesoporous metal–organic framework called NU-1000. *Nat. Protoc.* **2016**, *11*, 149–162.
- (31) Trickett, C. A.; Gagnon, K. J.; Lee, S.; Gándara, F.; Bürgi, H. B.; Yaghi, O. M. Definitive Molecular Level Characterization of Defects in UiO-66 Crystals. *Angew. Chem., Int. Ed.* **2015**, *54*, 11162–11167.
- (32) Yang, Q.; Jobic, H.; Salles, F.; Kolokolov, D.; Guiller, V.; Serre, C.; Maurin, G. Probing the dynamics of CO<sub>2</sub> and CH<sub>4</sub> within the porous zirconium terephthalate UiO-66(Zr): A synergic combination of neutron scattering measurements and molecular simulations. *Chem. - Eur. J.* **2011**, *17*, 8882–8889.
- (33) Taddei marcotaddei, M. & Scherrer Institut, P. UiO-66: a Case Study Metal-Organic Framework, 2016.
- (34) Kim, M.; Cahill, J. F.; Fei, H. H.; Prather, K. A.; Cohen, S. M. Postsynthetic Ligand and Cation Exchange in Robust Metal-Organic Frameworks. *J. Am. Chem. Soc.* **2012**, *134*, 18082–18088.
- (35) Bueken, B.; Krajnc, A.; Taulelle, F.; Bennett, T. D.; Smolders, S.; Mellot-Draznieks, C.; Mali, G.; Van Velthoven, N.; De Vos, D. Tackling the Defect Conundrum in UiO-66: A Mixed-Linker Approach to Engineering Missing Linker Defects. *Chem. Mater.* **2017**, *29*, 10478–10486.
- (36) Cliffe, M. J.; Wan, W.; Zou, X.; Chater, P. A.; Kleppe, A. K.; Tucker, M. G.; Wilhelm, H.; Funnell, N. P.; Coudert, F. X.; Goodwin, A. L. Correlated defect nanoregions in a metal–organic framework. *Nat. Commun.* **2014**, *5*, 1–8.
- (37) Shearer, G. C.; Chavan, S.; Ethiraj, J.; Vitillo, J. G.; Svelle, S.; Olsbye, U.; Lamberti, C.; Bordiga, S.; Lillerud, K. P. Tuned to Perfection: Ironing Out the Defects in Metal–Organic Framework UiO-66. *Chem. Mater.* **2014**, *26*, 4068–4071.
- (38) Thornton, A. W.; Babara, R.; Jain, A.; Trouselet, F.; Coudert, F. X. Defects in metal–organic frameworks: A compromise between adsorption and stability? *Dalt. Trans.* **2016**, *45*, 4352–4359.
- (39) Liu, L.; Chen, Z.; Wang, J.; Zhang, D.; Zhu, Y.; Ling, S.; Huang, K. W.; Belmabkhout, Y.; Adil, K.; Zhang, Y.; Slater, B.; Eddaoudi, M.; Han, Y. Imaging defects and their evolution in a metal–organic framework at sub-unit-cell resolution. *Nat. Chem.* **2019**, *11*, 622–628.
- (40) Shearer, G. C.; Chavan, S.; Bordiga, S.; Svelle, S.; Olsbye, U.; Lillerud, K. P. Defect Engineering: Tuning the Porosity and Composition of the Metal–Organic Framework UiO-66 via Modulated Synthesis. *Chem. Mater.* **2016**, *28*, 3749–3761.
- (41) Butova, V. V.; Budnyk, A. P.; Guda, A. A.; Lomachenko, K. A.; Bugaev, A. L.; Soldatov, A. V.; Chavan, S. M.; Øien-Ødegaard, S.; Olsbye, U.; Lillerud, K. P.; Atzori, C.; Bordiga, S.; Lamberti, C. Modulator effect in UiO-66-NDC (1, 4-naphthalenedicarboxylic acid) synthesis and comparison with UiO-67-NDC isoreticular metal–organic frameworks. *Cryst. Growth Des.* **2017**, *17*, 5422–5431.
- (42) Yuan, S.; Li, J.; Alsalmeh, A.; Feng, L.; Bosch, M.; Zou, L.; Huang, L.; Wang, X.; Zhou, H.-C.; Cagin, T.; Qin, J.-S. Construction of hierarchically porous metal–organic frameworks through linker labilization. *Nat. Commun.* **2017**, *8*, 15356.
- (43) Waitschat, S.; Fröhlich, D.; Reinsch, H.; Terraschke, H.; Lomachenko, K. A.; Lamberti, C.; Kummer, H.; Helling, T.; Baumgartner, M.; Henninger, S.; Stock, N. Synthesis of M-UiO-66 (M = Zr, Ce or Hf) employing 2,5-pyridinedicarboxylic acid as a linker: Defect chemistry, framework hydrophilisation and sorption properties. *Dalt. Trans.* **2018**, *47*, 1062–1070.
- (44) Diring, S.; Furukawa, S.; Takashima, Y.; Tsuruoka, T.; Kitagawa, S. Controlled multiscale synthesis of porous coordination polymer in nano/micro regimes. *Chem. Mater.* **2010**, *22*, 4531–4538.
- (45) Vermoortele, F.; Bueken, B.; Le Bars, G.; Van De Voorde, B.; Vandichel, M.; Houthoofd, K.; Vimont, A.; Daturi, M.; Waroquier, M.; Van Speybroeck, V.; Kirschhock, C.; De Vos, D. E. Synthesis modulation as a tool to increase the catalytic activity of metal–organic frameworks: The unique case of UiO-66(Zr). *J. Am. Chem. Soc.* **2013**, *135*, 11465–11468.

- (46) Vermoortele, F.; Ameloot, R.; Alaerts, L.; Matthessen, R.; Carlier, B.; Fernandez, E. V. R.; Gascon, J.; Kapteijn, F.; De Vos, D. E. Tuning the catalytic performance of metal-organic frameworks in fine chemistry by active site engineering. *J. Mater. Chem.* **2012**, *22*, 10313–10321.
- (47) Vandichel, M.; Hajek, J.; Vermoortele, F.; Waroquier, M.; De Vos, D. E.; Van Speybroeck, V. Active site engineering in UiO-66 type metal-organic frameworks by intentional creation of defects: A theoretical rationalization. *CrystEngComm* **2015**, *17*, 395–406.
- (48) Tcholakova, S.; Mitrova, Z.; Golemanov, K.; Denkov, N. D.; Vethamuthu, M.; Ananthapadmanabhan, K. P. Control of Ostwald ripening by using surfactants with high surface modulus. *Langmuir* **2011**, *27*, 14807–14819.
- (49) Miyamoto, M.; Kohmura, S.; Iwatsuka, H.; Oumi, Y.; Uemiyu, S. In situ solvothermal growth of highly oriented Zr-based metal organic framework UiO-66 film with monocrystalline layer. *CrystEngComm* **2015**, *17*, 3422–3425.
- (50) Hu, Z.; Nalaparaju, A.; Peng, Y.; Jiang, J.; Zhao, D. Modulated Hydrothermal Synthesis of UiO-66(Hf)-Type Metal-Organic Frameworks for Optimal Carbon Dioxide Separation. *Inorg. Chem.* **2016**, *55*, 1134–1141.
- (51) Lammert, M.; Wharmby, M. T.; Smolders, S.; Bueken, B.; Lieb, A.; Lomachenko, K. A.; De Vos, D.; Stock, N. Cerium-based metal organic frameworks with UiO-66 architecture: Synthesis, properties and redox catalytic activity. *Chem. Commun.* **2015**, *51*, 12578–12581.
- (52) Chavan, S. M.; Shearer, G. C.; Svelle, S.; Olsbye, U.; Bonino, F.; Ethiraj, J.; Lillerud, K. P.; Bordiga, S. Synthesis and characterization of amine-functionalized mixed-ligand metal-organic frameworks of UiO-66 topology. *Inorg. Chem.* **2014**, *53*, 9509–9515.
- (53) Taddei, M.; Tiana, D.; van Bokhoven, J. A.; Smit, B.; Casati, N.; Ranocchiari, M. Mixed-linker UiO-66: structure–property relationships revealed by a combination of high-resolution powder X-ray diffraction and density functional theory calculations. *Phys. Chem. Chem. Phys.* **2017**, *19*, 1551–1559.
- (54) Lee, Y.; Kim, S.; Kang, J. K.; Cohen, S. M. Photocatalytic CO<sub>2</sub> reduction by a mixed metal (Zr/Ti), mixed ligand metal-organic framework under visible light irradiation. *Chem. Commun.* **2015**, *51*, 5735–5738.
- (55) Jacobsen, J.; Reinsch, H.; Stock, N. Systematic Investigations of the Transition between Framework Topologies in Ce/Zr-MOFs. *Inorg. Chem.* **2018**, *57*, 12820–12826.
- (56) Chen, Z.; Hanna, S. L.; Redfern, L. R.; Alezi, D.; Islamoglu, T.; Farha, O. K. Reticular chemistry in the rational synthesis of functional zirconium cluster-based MOFs. *Coord. Chem. Rev.* **2019**, *386*, 32–49.
- (57) Hu, Z.; Peng, Y.; Kang, Z.; Qian, Y.; Zhao, D. A Modulated Hydrothermal (MHT) Approach for the Facile Synthesis of UiO-66-Type MOFs. *Inorg. Chem.* **2015**, *54*, 4862–4868.
- (58) Biswas, S.; Zhang, J.; Li, Z. B.; Liu, Y. Y.; Grzywa, M.; Sun, L. X.; Volkmer, D.; Van der Voort, P. Enhanced selectivity of CO<sub>2</sub> over CH<sub>4</sub> in sulfonate-, carboxylate- and iodo-functionalized UiO-66 frameworks. *Dalt. Trans.* **2013**, *42*, 4730–4737.
- (59) Zhao, W.; Zhang, C.; Yan, Z.; Zhou, Y.; Li, J.; Xie, Y.; Bai, L.; Jiang, L.; Li, F. Preparation, characterization, and performance evaluation of UiO-66 analogues as stationary phase in HPLC for the separation of substituted benzenes and polycyclic aromatic hydrocarbons. *PLoS One* **2017**, *12*, 1–13.
- (60) Peterson, G. W.; Moon, S. Y.; Wagner, G. W.; Hall, M. G.; Decoste, J. B.; Hupp, J. T.; Farha, O. K. Tailoring the Pore Size and Functionality of UiO-Type Metal-Organic Frameworks for Optimal Nerve Agent Destruction. *Inorg. Chem.* **2015**, *54*, 9684–9686.
- (61) Bugaev, A. L.; Guda, A. A.; Lomachenko, K. A.; Kamyshova, E. G.; Soldatov, M. A.; Kaur, G.; Øien-Ødegaard, S.; Braglia, L.; Lazzarini, A.; Manzoli, M.; Bordiga, S.; Olsbye, U.; Lillerud, K. P.; Soldatov, A. V.; Lamberti, C. Operando study of palladium nanoparticles inside UiO-67 MOF for catalytic hydrogenation of hydrocarbons. *Faraday Discuss.* **2018**, *208*, 287–306.
- (62) Katz, M. J.; Brown, Z. J.; Colón, Y. J.; Siu, P. W.; Scheidt, K. A.; Snurr, R. Q.; Hupp, J. T.; Farha, O. K. A facile synthesis of UiO-66, UiO-67 and their derivatives. *Chem. Commun.* **2013**, *49*, 9449–9451.
- (63) Ke, F.; Peng, C.; Zhang, T.; Zhang, M.; Zhou, C.; Cai, H.; Zhu, J.; Wan, X. Fumarate-based metal-organic frameworks as a new platform for highly selective removal of fluoride from brick tea. *Sci. Rep.* **2018**, *8*, 1–11.
- (64) Wißmann, G.; Schneider, A. M.; Behrens, P.; Lilienthal, S.; Bremer, I.; Schaate, A. Modulated synthesis of Zr-fumarate MOF. *Microporous Mesoporous Mater.* **2012**, *152*, 64–70.
- (65) Kim, M.; Cohen, S. M. Discovery, Development, and Functionalization of Zr(IV)-Based Metal–Organic Frameworks. *CrystEngComm* **2012**, *14*, 4096–4104.
- (66) Pang, J.; Yuan, S.; Qin, J.; Wu, M.; Lollar, C. T.; Li, J.; Huang, N.; Li, B.; Zhang, P.; Zhou, H. C. Enhancing Pore-Environment Complexity Using a Trapezoidal Linker: Toward Stepwise Assembly of Multivariate Quinary Metal-Organic Frameworks. *J. Am. Chem. Soc.* **2018**, *140*, 12328–12332.
- (67) Bueken, B.; Reinsch, H.; Reimer, N.; Stassen, I.; Vermoortele, F.; Ameloot, R.; Stock, N.; Kirschhock, C. E. A.; De Vos, D. A zirconium squarate metal-organic framework with modulator-dependent molecular sieving properties. *Chem. Commun. (Cambridge, U. K.)* **2014**, *50*, 10055–8.
- (68) DeSantis, D.; Mason, J. A.; James, B. D.; Houchins, C.; Long, J. R.; Veenstra, M. Techno-economic Analysis of Metal-Organic Frameworks for Hydrogen and Natural Gas Storage. *Energy Fuels* **2017**, *31*, 2024–2032.
- (69) Yang, Q.; Vaesen, S.; Ragon, F.; Wiersum, A. D.; Wu, D.; Lago, A.; Devic, T.; Martineau, C.; Taulelle, F.; Llewellyn, P. L.; Jobic, H.; Zhong, C.; Serre, C.; De Weireld, G.; Maurin, G. A water stable metal-organic framework with optimal features for CO<sub>2</sub> capture. *Angew. Chem., Int. Ed.* **2013**, *52*, 10316–10320.
- (70) Reinsch, H.; Bueken, B.; Vermoortele, F.; Stassen, I.; Lieb, A.; Lillerud, K. P.; De Vos, D. Green synthesis of zirconium-MOFs. *CrystEngComm* **2015**, *17*, 4070–4074.
- (71) Ragon, F.; Horcajada, P.; Chevreau, H.; Hwang, Y. K.; Lee, U. H.; Miller, S. R.; Devic, T.; Chang, J. S.; Serre, C. In situ energy-dispersive x-ray diffraction for the synthesis optimization and scale-up of the porous zirconium terephthalate UiO-66. *Inorg. Chem.* **2014**, *53*, 2491–2500.
- (72) Goesten, M. G.; de Lange, M. F.; Olivos-Suarez, A. I.; Bavykina, A. V.; Serra-Crespo, P.; Krywka, C.; Bickelhaupt, F. M.; Kapteijn, F.; Gascon, J. Evidence for a chemical clock in oscillatory formation of UiO-66. *Nat. Commun.* **2016**, *7*, No. 11832, DOI: 10.1038/ncomms11832.
- (73) Firth, F. C. N.; Cliffe, M. J.; Vulpe, D.; Aragonés-Anglada, M.; Moghadam, P. Z.; Fairen-Jimenez, D.; Slater, B.; Grey, C. P. Engineering new defective phases of UiO family metal-organic frameworks with water. *J. Mater. Chem. A* **2019**, *7*, 7459–7469.
- (74) Bai, Y.; Dou, Y.; Xie, L. H.; Rutledge, W.; Li, J. R.; Zhou, H. C. Zr-based metal-organic frameworks: Design, synthesis, structure, and applications. *Chem. Soc. Rev.* **2016**, *45*, 2327–2367.
- (75) Yuan, S.; Qin, J. S.; Lollar, C. T.; Zhou, H. C. Stable Metal-Organic Frameworks with Group 4 Metals: Current Status and Trends. *ACS Cent. Sci.* **2018**, *4*, 440–450.
- (76) Park, H.; Kim, S.; Jung, B.; Park, M. H.; Kim, Y.; Kim, M. Defect Engineering into Metal-Organic Frameworks for the Rapid and Sequential Installation of Functionalities. *Inorg. Chem.* **2018**, *57*, 1040–1047.
- (77) Ren, J.; Ledwaba, M.; Musyoka, N. M.; Langmi, H. W.; Mathe, M.; Liao, S.; Pang, W. Structural defects in metal–organic frameworks (MOFs): Formation, detection and control towards practices of interests. *Coord. Chem. Rev.* **2017**, *349*, 169–197.
- (78) Novoselov, K. S.; Geim, A. K.; Morozov, S. V.; Jiang, D.; Zhang, Y.; Dubonos, S. V.; Grigorieva, I. V.; Firsov, A. A. *Science* **2004**, *306*, 666–669.
- (79) Zhang, H. Ultrathin Two-Dimensional Nanomaterials. *ACS Nano* **2015**, *9*, 9451–9469.
- (80) Zhao, M.; Huang, Y.; Peng, Y.; Huang, Z.; Ma, Q.; Zhang, H. Two-dimensional metal-organic framework nanosheets: Synthesis and applications. *Chem. Soc. Rev.* **2018**, *47*, 6267–6295.



- (81) Peng, Y.; Li, Y.; Ban, Y.; Jin, H.; Jiao, W.; Liu, X.; Yang, W. Metal-organic framework nanosheets as building blocks for molecular sieving membranes. *Science (Washington, DC, U. S.)* **2014**, *346*, 1356–1359.
- (82) Rodenas, T.; Luz, I.; Prieto, G.; Seoane, B.; Miro, H.; Corma, A.; Kapteijn, F.; Llabrés i Xamena, F. X.; Gascon, J. Metal-organic framework nanosheets in polymer composite materials for gas separation. *Nat. Mater.* **2015**, *14*, 48–55.
- (83) Lee, J.; Farha, O. K.; Roberts, J.; Scheidt, K. A.; Nguyen, S. T.; Hupp, J. T. Metal-organic framework materials as catalysts. *Chem. Soc. Rev.* **2009**, *38*, 1450–1459.
- (84) Li, C.; Hu, X.; Tong, W.; Yan, W.; Lou, X.; Shen, M.; Hu, B. Ultrathin Manganese-Based Metal-Organic Framework Nanosheets: Low-Cost and Energy-Dense Lithium Storage Anodes with the Coexistence of Metal and Ligand Redox Activities. *ACS Appl. Mater. Interfaces* **2017**, *9*, 29829–29838.
- (85) Su, F.; Tian, J.-Y.; Ji, H.; Fang, S.; Liu, C.-S.; Zhu, X.; Zhang, Z.; Du, M.; Zhang, S.; Zhao, H. Two-Dimensional Zirconium-Based Metal–Organic Framework Nanosheet Composites Embedded with Au Nanoclusters: A Highly Sensitive Electrochemical Aptasensor toward Detecting Cocaine. *ACS Sensors* **2017**, *2*, 998–1005.
- (86) He, C.; Lu, K.; Liu, D.; Lin, W. Nanoscale metal-organic frameworks for the co-delivery of cisplatin and pooled siRNAs to enhance therapeutic efficacy in drug-resistant ovarian cancer cells. *J. Am. Chem. Soc.* **2014**, *136*, 5181–5184.
- (87) He, T.; Ni, B.; Zhang, S.; Gong, Y.; Wang, H.; Gu, L.; Zhuang, J.; Hu, W.; Wang, X. Ultrathin 2D Zirconium Metal–Organic Framework Nanosheets: Preparation and Application in Photocatalysis. *Small* **2018**, *14*, 10–15.
- (88) Wang, Y.; Li, L.; Yan, L.; Gu, X.; Dai, P.; Liu, D.; Bell, J. G.; Zhao, G.; Zhao, X.; Thomas, K. M. Bottom-Up Fabrication of Ultrathin 2D Zr Metal-Organic Framework Nanosheets through a Facile Continuous Microdroplet Flow Reaction. *Chem. Mater.* **2018**, *30*, 3048–3059.
- (89) Zhang, X.; Zhang, P.; Chen, C.; Zhang, J.; Yang, G.; Zheng, L.; Zhang, J.; Han, B. Fabrication of 2D metal–organic framework nanosheets with tailorable thickness using bio-based surfactants and their application in catalysis. *Green Chem.* **2019**, *21*, 54–58.
- (90) Cao, L.; Lin, Z.; Shi, W.; Wang, Z.; Zhang, C.; Hu, X.; Wang, C.; Lin, W. Exciton Migration and Amplified Quenching on Two-Dimensional Metal-Organic Layers. *J. Am. Chem. Soc.* **2017**, *139*, 7020–7029.
- (91) Cliffe, M. J.; Castillo-Martinez, E.; Wu, Y.; Lee, J.; Forse, A. C.; Firth, F. C. N.; Moghadam, P. Z.; Fairen-Jimenez, D.; Gaultois, M. W.; Hill, J. A.; Magdysyuk, O. V.; Slater, B.; Goodwin, A. L.; Grey, C. P. Metal-Organic Nanosheets Formed via Defect-Mediated Transformation of a Hafnium Metal-Organic Framework. *J. Am. Chem. Soc.* **2017**, *139*, 5397–5404.
- (92) Cao, L.; Lin, Z.; Peng, F.; Wang, W.; Huang, R.; Wang, C.; Yan, J.; Liang, J.; Zhang, Z.; Zhang, T.; Long, L.; Sun, J.; Lin, W. Self-Supporting Metal-Organic Layers as Single-Site Solid Catalysts. *Angew. Chem., Int. Ed.* **2016**, *55*, 4962–4966.
- (93) Petit, C. Present and future of MOF research in the field of adsorption and molecular separation. *Curr. Opin. Chem. Eng.* **2018**, *20*, 132–142.
- (94) Yaghi, O. M.; Trickett, C. A.; Helal, A.; Al-Maythaly, B. A.; Yamani, Z. H.; Cordova, K. E. The chemistry of metal–organic frameworks for CO<sub>2</sub> capture, regeneration and conversion. *Nat. Rev. Mater.* **2017**, *2*, 17045.
- (95) Mounfield, W. P.; Han, C.; Pang, S. H.; Tumuluri, U.; Jiao, Y.; Bhattacharyya, S.; Dutzer, M. R.; Nair, S.; Wu, Z.; Lively, R. P.; Sholl, D. S.; Walton, K. S. Synergistic effects of water and SO<sub>2</sub> on degradation of MIL-125 in the presence of acid gases. *J. Phys. Chem. C* **2016**, *120*, 27230–27240.
- (96) Barea, E.; Montoro, C.; Navarro, J. A. R. Toxic gas removal-metal-organic frameworks for the capture and degradation of toxic gases and vapours. *Chem. Soc. Rev.* **2014**, *43*, 5419–5430.
- (97) Rieth, A. J.; Tulchinsky, Y.; Dincă, M. High and Reversible Ammonia Uptake in Mesoporous Azolate Metal-Organic Frameworks with Open Mn, Co, and Ni Sites. *J. Am. Chem. Soc.* **2016**, *138*, 9401–9404.
- (98) Shah, M. S.; Tsapatsis, M.; Siepmann, J. I. Hydrogen Sulfide Capture: From Absorption in Polar Liquids to Oxide, Zeolite, and Metal-Organic Framework Adsorbents and Membranes. *Chem. Rev.* **2017**, *117*, 9755–9803.
- (99) Yang, S. H.; Rao, S. R.; Narayanan, S.; Kapustin, E. A.; Furukawa, H.; Umans, A. S.; Yaghi, O. M.; Wang, E. N. Powered By Natural Sunlight. *Science (80-.)* **2017**, *434*, 430–434.
- (100) Dinca, M.; Dailly, A.; Liu, Y.; Brown, C. M.; Neumann, D. A.; Long, J. R. Hydrogen storage in a microporous metal-organic framework with exposed Mn<sup>2+</sup> coordination sites. *J. Am. Chem. Soc.* **2006**, *128*, 16876–16883.
- (101) Lin, J. M.; He, C. T.; Liu, Y.; Liao, P. Q.; Zhou, D. D.; Zhang, J. P.; Chen, X. M. A Metal-Organic Framework with a Pore Size/Shape Suitable for Strong Binding and Close Packing of Methane. *Angew. Chem., Int. Ed.* **2016**, *55*, 4674–4678.
- (102) Bloch, E. D.; Murray, L. J.; Queen, W. L.; Chavan, S.; Maximoff, S. N.; Bigi, J. P.; Krishna, R.; Peterson, V. K.; Grandjean, F.; Long, G. J.; Smit, B.; Bordiga, S.; Brown, C. M.; Long, J. R. Selective binding of O<sub>2</sub> over N<sub>2</sub> in a redox-active metal-organic framework with open iron(II) coordination sites. *J. Am. Chem. Soc.* **2011**, *133*, 14814–14822.
- (103) Bachman, J. E.; Kapelewski, M. T.; Reed, D. A.; Gonzalez, M. I.; Long, J. R. M<sub>2</sub>(m-dobdc) (M = Mn, Fe, Co, Ni) Metal-Organic Frameworks as Highly Selective, High-Capacity Adsorbents for Olefin/Paraffin Separations. *J. Am. Chem. Soc.* **2017**, *139*, 15363–15370.
- (104) Banerjee, D.; Simon, C. M.; Plonka, A. M.; Motkuri, R. K.; Liu, J.; Chen, X.; Smit, B.; Parise, J. B.; Haranczyk, M.; Thallapally, P. K. Metal-organic framework with optimally selective xenon adsorption and separation. *Nat. Commun.* **2016**, *7*, 1–7.
- (105) Wang, C.; Liu, X.; Keser Demir, N.; Chen, J. P.; Li, K. Applications of water stable metal-organic frameworks. *Chem. Soc. Rev.* **2016**, *45*, 5107–5134.
- (106) Zhang, T.; Lin, W. Metal-organic frameworks for artificial photosynthesis and photocatalysis. *Chem. Soc. Rev.* **2014**, *43*, 5982–5993.
- (107) Kim, S. N.; Lee, Y. R.; Hong, S. H.; Jang, M. S.; Ahn, W. S. Pilot-scale synthesis of a zirconium-benzenedicarboxylate UiO-66 for CO<sub>2</sub> adsorption and catalysis. *Catal. Today* **2015**, *245*, 54–60.
- (108) Rechac, V. L.; Cirujano, F. G.; Corma, A.; Llabrés i Xamena, F. X. Diastereoselective Synthesis of Pyranoquinolines on Zirconium-Containing UiO-66 Metal-Organic Frameworks. *Eur. J. Inorg. Chem.* **2016**, *2016*, 4512–4516.
- (109) Valekar, A. H.; Cho, K. H.; Chitale, S. K.; Hong, D. Y.; Cha, G. Y.; Lee, U. H.; Hwang, D. W.; Serre, C.; Chang, J. S.; Hwang, Y. K. Catalytic transfer hydrogenation of ethyl levulinate to  $\gamma$ -valerolactone over zirconium-based metal-organic frameworks. *Green Chem.* **2016**, *18*, 4542–4552.
- (110) Corma, A.; Iborra, S.; Velty, A. Chemical routes for the transformation of biomass into chemicals. *Chem. Rev.* **2007**, *107*, 2411–2502.
- (111) Kuwahara, Y.; Kango, H.; Yamashita, H. Catalytic Transfer Hydrogenation of Biomass-Derived Levulinic Acid and Its Esters to  $\gamma$ -Valerolactone over Sulfonic Acid-Functionalized UiO-66. *ACS Sustainable Chem. Eng.* **2017**, *5*, 1141–1152.
- (112) Miao, Z.; Qi, C.; Wensley, A. M.; Luan, Y. Development of a novel Brønsted acid UiO-66 metal-organic framework catalyst by postsynthetic modification and its application in catalysis. *RSC Adv.* **2016**, *6*, 67226–67231.
- (113) Ghorbani-Vaghei, R.; Azarifar, D.; Daliran, S.; Oveisi, A. R. The UiO-66-SO<sub>3</sub>H metal-organic framework as a green catalyst for the facile synthesis of dihydro-2-oxypyrrrole derivatives. *RSC Adv.* **2016**, *6*, 29182–29189.
- (114) Cirujano, F. G.; Corma, A.; Llabrés i Xamena, F. X. Conversion of levulinic acid into chemicals: Synthesis of biomass derived levulinate esters over Zr-containing MOFs. *Chem. Eng. Sci.* **2015**, *124*, 52–60.

- (115) Blandez, J. F.; Santiago-Portillo, A.; Navalón, S.; Giménez-Marqués, M.; Alvaro, M.; Horcajada, P.; García, H. Influence of functionalization of terephthalate linker on the catalytic activity of UiO-66 for epoxide ring opening. *J. Mol. Catal. A: Chem.* **2016**, *425*, 332–339.
- (116) Li, Y.; Xiao, A. S.; Zou, B.; Zhang, H. X.; Yan, K.; Lin, Y. Advances of metal–organic frameworks for gas sensing. *Polyhedron* **2018**, *154*, 83–97.
- (117) Horcajada, P.; Maurin, G.; Serre, C.; Allan, P. K.; Couvreur, P.; Férey, G.; Gref, R.; Baati, T.; Morris, R. E. Metal–Organic Frameworks in Biomedicine. *Chem. Rev.* **2012**, *112*, 1232–1268.
- (118) Peterson, G. W.; Destefano, M. R.; Garibay, S. J.; Ploskonka, A.; McEntee, M.; Hall, M.; Karwacki, C. J.; Hupp, J. T.; Farha, O. K. Optimizing Toxic Chemical Removal through Defect-Induced UiO-66-NH<sub>2</sub>Metal–Organic Framework. *Chem. - Eur. J.* **2017**, *23*, 15913–15916.
- (119) Peterson, G. W.; Decoste, J. B.; Fatollahi-Fard, F.; Britt, D. K. Engineering UiO-66-NH<sub>2</sub> for toxic gas removal. *Ind. Eng. Chem. Res.* **2014**, *53*, 701–707.
- (120) Mondloch, J. E.; Hupp, J. T.; Ghosh, P.; Peterson, G. W.; Cramer, C. J.; Isley, W. C., III; DeCoste, J. B.; Bury, W.; Hall, M. G.; Farha, O. K.; Wagner, G. W.; Liao, P.; Katz, M. J.; Snurr, R. Q. Destruction of chemical warfare agents using metal–organic frameworks. *Nat. Mater.* **2015**, *14*, 512–516.
- (121) Bobbitt, N. S.; Snurr, R. Q.; Farha, O. K.; Islamoglu, T.; Hupp, J. T.; Howarth, A. J.; Mendonca, M. L. Metal–organic frameworks for the removal of toxic industrial chemicals and chemical warfare agents. *Chem. Soc. Rev.* **2017**, *46*, 3357–3385.
- (122) DeCoste, J. B.; Peterson, G. W. Metal–Organic Frameworks for Air Purification of Toxic Chemicals. *Chem. Rev.* **2014**, *114*, 5695–5727.
- (123) Liu, Y.; Howarth, A. J.; Vermeulen, N. A.; Moon, S.-Y.; Hupp, J. T.; Farha, O. K. Catalytic Degradation of Chemical Warfare Agents and Their Simulants by Metal–Organic Frameworks. *Coord. Chem. Rev.* **2017**, *346*, 101.
- (124) Zou, D.; Liu, D. Understanding the modifications and applications of highly stable porous frameworks via UiO-66. *Mater. Today Chem.* **2019**, *12*, 139–165.
- (125) Min, X.; Wu, X.; Shao, P.; Ren, Z.; Ding, L.; Luo, X. Ultra-high capacity of lanthanum-doped UiO-66 for phosphate capture: Unusual doping of lanthanum by the reduction of coordination number. *Chem. Eng. J.* **2019**, *358*, 321–330.
- (126) Cao, J.; Yang, Z.-h.; Xiong, W.-p.; Zhou, Y.-y.; Peng, Y.-r.; Li, X.; Zhou, C.-y.; Xu, R.; Zhang, Y.-r. One-step synthesis of Co-doped UiO-66 nanoparticle with enhanced removal efficiency of tetracycline: Simultaneous adsorption and photocatalysis. *Chem. Eng. J.* **2018**, *353*, 126–137.
- (127) Han, Y.; Liu, M.; Li, K.; Sun, Q.; Zhang, W.; Song, C.; Zhang, G.; Conrad Zhang, Z.; Guo, X. In situ synthesis of titanium doped hybrid metal-organic framework UiO-66 with enhanced adsorption capacity for organic dyes. *Inorg. Chem. Front.* **2017**, *4*, 1870–1880.
- (128) Wen, M.; Mori, K.; Kuwahara, Y.; Yamashita, H. Plasmonic Au@Pd nanoparticles supported on a basic metal-organic framework: Synergic boosting of H<sub>2</sub> production from formic acid. *ACS Energy Lett.* **2017**, *2*, 1–7.
- (129) Yang, Y.; Liu, X.; Yan, D.; Deng, P.; Guo, Z.; Zhan, H. Europium ion post-functionalized zirconium metal-organic frameworks as luminescent probes for effectively sensing hydrazine hydrate. *RSC Adv.* **2018**, *8*, 17471–17476.
- (130) Xu, X. Y.; Yan, B. Eu(III) functionalized Zr-based metal-organic framework as excellent fluorescent probe for Cd<sup>2+</sup> detection in aqueous environment. *Sens. Actuators, B* **2016**, *222*, 347–353.
- (131) Yang, Z.; Xu, X.; Liang, X.; Lei, C.; Gao, L.; Hao, R.; Lu, D.; Lei, Z. Fabrication of Ce doped UiO-66/graphene nanocomposites with enhanced visible light driven photoactivity for reduction of nitroaromatic compounds. *Appl. Surf. Sci.* **2017**, *420*, 276–285.
- (132) Yang, J. M.; Ying, R. J.; Han, C. X.; Hu, Q. T.; Xu, H. M.; Li, J. H.; Wang, Q.; Zhang, W. Adsorptive removal of organic dyes from aqueous solution by a Zr-based metal-organic framework: Effects of Ce(III) doping. *Dalt. Trans.* **2018**, *47*, 3913–3920.
- (133) Ebrahim, A. M.; Bandoz, T. J. Ce(III) doped Zr-based MOFs as excellent NO<sub>2</sub> adsorbents at ambient conditions. *ACS Appl. Mater. Interfaces* **2013**, *5*, 10565–10573.